JGR Solid Earth

RESEARCH ARTICLE
10.1029/2023JB027493

Tectono-Stratigraphic Evolution of the Kerguelen Large Igneous Province: The Conjugate William's Ridge-Broken Ridge Rifted Margins

L. Magri[1,2], J. M. Whittaker[1], M. F. Coffin[1,3,4], K. Hochmuth[1,2], D. Gürer[1,5], S. Williams[1], G. Bernardel[6], and G. Uenzelmann-Neben[7]

[1]Institute for Marine and Antarctic Studies, University of Tasmania, Hobart, TAS, Australia, [2]Australian Centre for Excellence in Antarctic Sciences, University of Tasmania, Hobart, TAS, Australia, [3]School of Earth and Climate Sciences, University of Maine, Orono, ME, USA, [4]Department of Geology and Geophysics, Woods Hole Oceanographic Institution, Woods Hole, MA, USA, [5]School of the Environment, The University of Queensland, St. Lucia, QLD, Australia, [6]Geoscience Australia, Canberra, ACT, Australia, [7]Alfred-Wegener-Institut Helmholtz-Zentrum für Polar- und Meeresforschung, Bremerhaven, Germany

Abstract Extensive investigation of continental rift systems has been fundamental for advancing the understanding of extensional tectonics and modes of formation of new ocean basins. However, current rift classification schemes do not account for conjugate end members formed by Large Igneous Province crust, referring to thick mafic crust, sometimes including continental fragments. Here, we investigate the rifting of William's Ridge (Kerguelen Plateau) and Broken Ridge, components of the Kerguelen Large Igneous Province now situated in the Southeast Indian Ocean, and incorporate these end members into the deformation migration concept for rifted margins. We use multichannel seismic reflection profiles and data from scientific drill cores acquired on both conjugate margins to propose, for the first time, a combined tectono-stratigraphic framework. We interpret seismic patterns, tectonic features, and magnetic anomaly picks to determine an across-strike structural domain classification. This interpretation considers the rift system overall to be "magma-poor" despite being located proximal to the Kerguelen plume but suggests that syn-rift interaction between the Kerguelen mantle plume and the lithospheric structure of William's Ridge and Broken Ridge has controlled the along-strike segmentation of both conjugates. We integrate seismic reflection and bathymetric data to test the hypothesis of predominantly transform motion, between the Australian and Antarctic plates, in Late Cretaceous and Paleogene time.

Plain Language Summary Numerous investigations into the evolution of continental rift systems have advanced understanding of how the Earth's crust stretches and may eventually result in the formation of new ocean basins. However, these studies have not considered the case of thick mafic crust, sometimes including continental fragments. Here we focus on William's Ridge (Kerguelen Plateau) and Broken Ridge, formed as a single feature, in the Southern Indian Ocean. We investigate how these features rifted, broke apart, and separated in the current conceptual framework of deformation migration. We use multichannel seismic reflection data, multibeam bathymetry data, drilling results, and magnetics data to interpret their structure, stratigraphy, and tectonics with the goal of explaining how the features evolved in time and space. Surprisingly, we find evidence for relatively weak magmatism despite the features being located near a mantle hotspot. Nevertheless, we suggest that the mantle hotspot influenced how the crust broke apart along different segments of the features' conjugate margins. We also find that the Australia and Antarctic tectonic plates, on which the features are now located, were moving laterally with respect to each other while rifting and breaking apart.

Key Points:

- The first consistent tectono-stratigraphic framework across the Kerguelen Plateau-Broken Ridge rifted margins is presented
- William's Ridge-Broken Ridge rifted margins are defined as "magma-poor" and classified following the deformation migration model
- The Kerguelen mantle plume controls along-strike segmentation and promotes syn-rift transform motion in William's Ridge-Broken Ridge

Supporting Information:

Supporting Information may be found in the online version of this article.

Correspondence to:

L. Magri,
Luca.Magri@utas.edu.au

Citation:

Magri, L., Whittaker, J. M., Coffin, M. F., Hochmuth, K., Gürer, D., Williams, S., et al. (2024). Tectono-stratigraphic evolution of the Kerguelen Large Igneous Province: The conjugate William's Ridge-Broken Ridge rifted margins. *Journal of Geophysical Research: Solid Earth*, *129*, e2023JB027493. https://doi.org/10.1029/2023JB027493

Received 19 JULY 2023
Accepted 14 FEB 2024

Author Contributions:

Conceptualization: L. Magri, J. M. Whittaker, M. F. Coffin, K. Hochmuth
Data curation: L. Magri, J. M. Whittaker, M. F. Coffin, G. Uenzelmann-Neben
Formal analysis: L. Magri
Funding acquisition: J. M. Whittaker, M. F. Coffin, G. Bernardel, G. Uenzelmann-Neben
Investigation: L. Magri, J. M. Whittaker, M. F. Coffin, D. Gürer, G. Bernardel, G. Uenzelmann-Neben

1. Introduction

Extensional tectonic processes have been well studied in continental and oceanic settings leading to advanced understanding of continental rifting, lithospheric stretching, and the modes of formation of new ocean basins. Rifted continental margins are usually described through a classification in dichotomies such as "magma-rich"-"magma-poor" rifted margin types (Peron-Pinvidic & Manatschal, 2019). More recent observations defined the concept of deformation migration (Peron-Pinvidic et al., 2013), where continental rifted margins are thought to respond to extensional stresses by episodically migrating oceanward. Research on extensional systems has been predominantly focussed on continental crust configurations, from the shallow water areas defining the edges

Methodology: L. Magri, J. M. Whittaker, M. F. Coffin, K. Hochmuth, D. Gürer, G. Bernardel, G. Uenzelmann-Neben
Project administration: L. Magri, J. M. Whittaker, M. F. Coffin, K. Hochmuth
Resources: J. M. Whittaker, M. F. Coffin, G. Bernardel
Software: L. Magri, J. M. Whittaker, K. Hochmuth
Supervision: J. M. Whittaker, M. F. Coffin, K. Hochmuth, D. Gürer, S. Williams
Visualization: L. Magri, J. M. Whittaker, M. F. Coffin, K. Hochmuth, D. Gürer, S. Williams, G. Bernardel, G. Uenzelmann-Neben
Writing – original draft: L. Magri
Writing – review & editing: L. Magri, J. M. Whittaker, M. F. Coffin, K. Hochmuth, D. Gürer, S. Williams, G. Uenzelmann-Neben

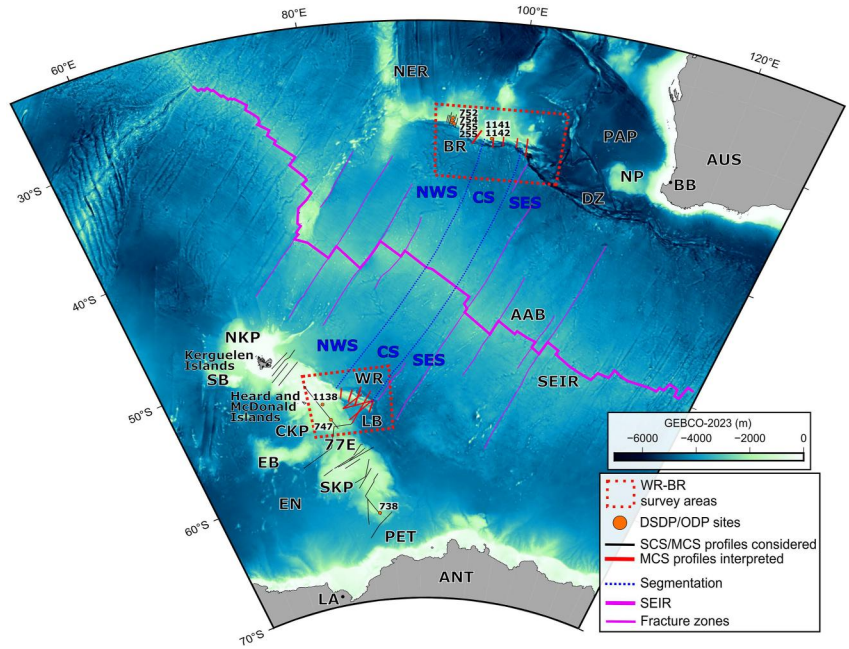

Figure 1. GEBCO, 2023 gridded bathymetric map (GEBCO, 2023) of the Southern Indian Ocean, Kerguelen Plateau-Broken Ridge region. Coastlines—thin black lines; landmasses—gray shading. Red dotted boxes indicate the two study areas (William's Ridge and Broken Ridge). Medium black lines represent a subset of single channel seismic reflection (SCS) and multichannel seismic reflection (MCS) profiles considered in this study. Thick red lines represent MCS profiles analyzed in this study. Orange dots show Deep Sea Drilling Project and Ocean Drilling Program sites within the two study areas. Thick purple line is the Southeast Indian Ridge (SEIR), and medium purple lines are the fracture zones in the Kerguelen Plateau-Broken Ridge sector. Blue dotted lines represent the conjugate segmentation of the William's Ridge-Broken Ridge area. AAB, Australian-Antarctic Basin; ANT, Antarctica; AUS, Australia; BB, Bunbury Basalts; BR, Broken Ridge; CKP, Central Kerguelen Plateau; CS, Central segment; DZ, Diamantina Zone; EB, Elan Bank; EN, Enderby Basin; LA, lamprophyres; LB, Labuan Basin; NER, Ninetyeast Ridge; NKP, Northern Kerguelen Plateau; NP, Naturaliste Plateau; NWS, Northwest segment; PAP, Perth Abyssal Plain; PET, Princess Elizabeth Trough; SB, Skiff Bank; SEIR, Southeast Indian Ridge; SES, Southeast segment; SKP, Southern Kerguelen Plateau; WR, William's Ridge; 77° East Graben. Additional lamprophyres and Rajmahal are located on the Indian subcontinent (Coffin et al., 2002).

of the continents to the far offshore oceanic zones (Peron-Pinvidic & Manatschal, 2019; Reston, 2009), and oceanic systems targeting the evolution of mid-ocean ridges (Dick et al., 2003; Schierjott et al., 2023). However, how extensional processes occur in Large Igneous Provinces (LIPs), which is distinct from both continental and oceanic lithosphere, remains entirely unknown.

One good example of the discrepancy in knowledge between extensional processes in continental and LIP lithosphere is the rift system between Australia and Antarctica which, over the last decade, has been described by several studies involving the analysis of multichannel seismic reflection (MCS) data (e.g., Gillard et al., 2015; Sauermilch et al., 2019). Although fundamental for improving the general understanding on rifting, breakup and geometry of the continental sectors of the Australian-Antarctic rift systems, these studies lack a detailed explanation of rifting modes in the westernmost sector of the Australian-Antarctic boundary (Whittaker et al., 2013), which ran through the Kerguelen LIP (Coffin & Eldholm, 1994; Coffin et al., 2002). In this study, we focus on how the extension and breakup of the Kerguelen LIP occurred, particularly the evolution of the conjugate William's Ridge, in Kerguelen Plateau, and Broken Ridge. We analyze these conjugate, dominantly mafic end members of the rift system, separated by seafloor spreading along the Southeast Indian Ridge (SEIR, Figure 1) (Mutter & Cande, 1983; Royer & Coffin, 1992; Tikku & Cande, 2000; Whittaker et al., 2013), to create the first integrated tectono-stratigraphic framework of extension in a LIP setting.

The entire William's Ridge-Broken Ridge system was likely influenced by the Kerguelen mantle plume during rifting and breakup, based on existing plate tectonic reconstructions (Whittaker et al., 2013) in a hotspot reference frame (O'Neill et al., 2005) and assuming a hotspot radius of influence of ~1,400 km (Campbell & Griffiths, 1990; Griffiths & Campbell, 1991; Hill et al., 1992; Whittaker et al., 2015). The relationship between the

Kerguelen mantle plume and the Australian-Antarctic tectonic plates was considered at a regional scale by Whittaker et al. (2013), who proposed interaction between the Kerguelen mantle plume and the SEIR, tracking through the conjoined Kerguelen Plateau/William's Ridge/Broken Ridge for at least ∼65 Myr until breakup at ∼44 Ma (Tikku & Cande, 2000). Here, we investigate and unravel this interaction in more detail using satellite-derived and multibeam bathymetric data, along with legacy seismic reflection data and new MCS profiles.

Rift systems evolving in the vicinity of a mantle plume are understood to manifest through the emplacement of thick oceanic crust (Geoffroy, 2005; Hochmuth et al., 2019; White & McKenzie, 1989; White et al., 1987), often composed by seaward dipping reflection sequences (SDRs) (Backman et al., 1984; Callot et al., 2002; Geoffroy, 2005; Hinz, 1981; Mutter et al., 1982). This evidence, typically associated with narrow rift systems, is required to assign conjugate margins the classification of "magma-rich" (Geoffroy, 2005; Peron-Pinvidic & Manatschal, 2019; Tomasi et al., 2021). This nomenclature contrasts with "magma-poor" rifted margins, which are thought to be characterized by minor presence of magmatic material and a broader zone of lithospheric thinning (Biari et al., 2021; T. Doré & Lundin, 2015; Franke, 2013; Lavier & Manatschal, 2006; Manatschal, 2004; Peron-Pinvidic & Manatschal, 2019; Sutra & Manatschal, 2012). A complementary rift systems classification concept is the deformation migration paradigm (Peron-Pinvidic et al., 2013), which has been remarkably valuable for improving the understanding of the evolution of the lithosphere, in response to active and passive mantle dynamics (Geoffroy, 2005). However, a common feature characterizing every rift system classified under this paradigm is the predominantly continental nature of the crust. Considering that extensional deformation has been observed at several LIPs including Kerguelen (Coffin et al., 2002; Whittaker et al., 2013), Hikurangi-Manihiki (Davy et al., 2008; Hochmuth et al., 2015; Pietsch & Uenzelmann-Neben, 2015), Shatsky Rise (Nakanishi et al., 1999), Agulhas Plateau-Northeast Georgia Rise-Maud Rise (Gohl et al., 2011; Parsiegla et al., 2008; Uenzelmann-Neben et al., 1999), Rio Grande Rise-Walvis Ridge (Graça et al., 2019; Hoyer et al., 2022), in this paper we attempt to understand rift processes that affect LIP crust. We use the term LIP crust referring to thick mafic crust, sometimes including continental fragments, indicating pre-rift crustal thicknesses exclusively. We interpret the William's Ridge-Broken Ridge conjugate pair in the context of rifted margins deformation migration model (Peron-Pinvidic et al., 2013), assessing how well this model fits our study region and what adaptations may need to be made for LIP and possibly normal oceanic crustal settings.

2. Geological Setting

2.1. The Kerguelen Plateau-Broken Ridge System

The Kerguelen hotspot is associated with massive volcanism, outpouring since at least 130 Ma continuously, at different rates (Coffin et al., 2002), ∼2.5 × 10^7 km^3 of material to emplace the Kerguelen LIP (Borissova et al., 2002; Coffin et al., 2002; Walker & Geissman, 2022). The Kerguelen LIP encompasses extrusive and intrusive rocks emplaced both in oceans and on continents. Terrestrial rocks include the Rajmahal Traps in India, lamprophyres in India and Antarctica, and Bunbury Basalts in Australia (Argus et al., 2011; Coffin et al., 2002; DeMets et al., 2010). In the ocean are Broken Ridge, on the Australian plate, Ninetyeast Ridge on the Capricorn plate, and Elan Bank, Skiff Bank, Kerguelen Plateau (Northern Kerguelen Plateau, NKP; Central Kerguelen Plateau, CKP; Southern Kerguelen Plateau, SKP), on the Antarctic plate (Argus et al., 2011; Coffin et al., 2002; DeMets et al., 2010) (Figure 1). William's Ridge is located in the central part of the CKP (Coffin et al., 1986). Active volcanism on Heard and McDonalds Islands, Quaternary volcanism elsewhere on the CKP (Duncan et al., 2016), and Quaternary volcanism on the Kerguelen Islands (Bénard et al., 2010), document that the hotspot has been active in Quaternary time (Figure 1).

The Kerguelen Plateau and Broken Ridge have been investigated geophysically and geologically since the 1970s. Single channel seismic reflection (SCS) and MCS data were acquired by USNS *Eltanin* (Houtz et al., 1977), RV *Rig Seismic* (Borissova et al., 2002; Coffin et al., 1986; Ramsay et al., 1986), RV *Marion Dufresne* (Munschy, Fritsch, et al., 1992; Schlich et al., 1988), and RV *Robert D. Conrad* (Driscoll et al., 1991). Basement and sediment cores were drilled by DV *Glomar Challenger* through the Deep Sea Drilling Project (DSDP) (Davies et al., 1974) and by DV *JOIDES Resolution* through the Ocean Drilling Program (ODP) (Barron et al., 1989, 1991; Coffin et al., 2000; Frey et al., 2003; Peirce et al., 1989; Schlich et al., 1989; Weissel et al., 1991; Wise et al., 1992).

While initial studies of the Kerguelen Plateau and Broken Ridge (e.g., Houtz et al., 1977) contributed to Indian Ocean plate reconstructions (e.g., Norton & Molnar, 1977), the crustal nature of the Kerguelen Plateau and

Broken Ridge has remained somewhat enigmatic. Cores bearing tholeiitic basalts (Duncan, 2002; Jiang et al., 2021) underlying siliceous and carbonate sediment and sedimentary rocks have been drilled consistently on both Kerguelen Plateau and Broken Ridge (Barron et al., 1989; Coffin et al., 2000; Frey et al., 2003; Peirce et al., 1989; Schlich et al., 1989). Seismic refraction work (Operto & Charvis, 1996) and scientific ocean drilling (Coffin et al., 2000; Frey et al., 2003) strongly suggested and confirmed, respectively, the presence of continental crust within the KP. Seismic reflection and refraction data, gravity data, and subsidence modeling on the Kerguelen Plateau, and seismic refraction profiles acquired on Broken Ridge reveal the maximum crustal thickness of the two features to be ∼25 and ∼15 km, respectively (Charvis et al., 1995; Gladczenko & Coffin, 2001; MacKenzie et al., 1980; Operto & Charvis, 1995, 1996), thinning toward their edges (Coffin & Eldholm, 1994). The maximum crustal thickness of William's Ridge has been modeled to be 15 km (Gladczenko & Coffin, 2001).

William's Ridge and Broken Ridge were emplaced contiguously, and partially subaerially, due to massive volcanism between ∼93 and 109 and ∼98–99 Ma, respectively (Barron et al., 1989, 1991; Coffin et al., 2000; Davies et al., 1974; Frey et al., 2003; Jiang et al., 2021; Peirce et al., 1989; Schlich et al., 1989; Weissel et al., 1991; Wise et al., 1992). After emplacement, they subsided and became shallow-water carbonate platforms (Coffin, 1992; Munschy, Fritsch, et al., 1992; Wallace et al., 2002). In the early Maastrichtian, renewed tectonism resulted in uplift, which led to further subaerial conditions on Broken Ridge and formation of the 77°E Graben in the CKP (Driscoll et al., 1991; Munschy, Fritsch, et al., 1992). Following further brief subsidence, early Paleogene uplift, attributed to rift onset, culminated in the breakup of William's Ridge and Broken Ridge (Driscoll et al., 1991; Munschy & Schlich, 1987; Munschy, Fritsch, et al., 1992; Mutter & Cande, 1983). Broken Ridge has been proposed to be the footwall of the asymmetric rift system (Karner & Driscoll, 1993). Therefore, this end member is likely to have experienced a higher degree of rotation compared to William's Ridge, as numerical models suggest this to be the typical flexural response of the lower plate in normal fault settings (Buck, 1988, 2007; Lavier et al., 1999; Lister et al., 1986; Sandiford et al., 2021).

Together with episodes of uplift and subsidence, the evolution of the Kerguelen Plateau-Broken Ridge system has been significantly impacted by regional tectonic forces, controlled by horizontal stresses, in the framework of an evolving plate boundary. Plate motions in the Kerguelen sector can be modeled using magnetic anomaly and fracture zone identifications across the broader plate pair (Cande & Mutter, 1982; Munschy, 1998; Royer & Coffin, 1992; Tikku & Cande, 1999, 2000; Whittaker et al., 2013). The Kerguelen LIP emplacement largely occurred in an oceanic setting during a first rifting phase encompassing Early Cretaceous seafloor spreading between India and the then contiguous Australian-Antarctic system (Whittaker et al., 2013). During formation of the then continuous William's Ridge and Broken Ridge, a major plate tectonic reorganization, between 100 and 105 Ma, led to significant changes in relative plate motions among India, Australia, and Antarctica (Matthews et al., 2012). The major reorganization resulted in a progressive change from transtensional motion to almost purely strike-slip in the westernmost extent of the Australian-Antarctic plate boundary (Whittaker et al., 2013; Figure S1 in Supporting Information S1). This relative motion corresponded to a second rifting phase, largely orthogonal to first one, which was relatively consistent through Late Cretaceous and Early Paleogene time until a spreading center jump at ∼44 Ma, resulting in the breakup and separation of William's Ridge and Broken Ridge (Tikku & Cande, 2000; Whittaker et al., 2013) (Figure S1 in Supporting Information S1).

The Labuan Basin and Diamantina Zone extend eastward from the William's Ridge and Broken Ridge areas, respectively. Differences in depth to basement and sediment thicknesses between the Labuan Basin and the Australian-Antarctic Basin (Figure 1) led to the idea that the former formed by rifting starting at ∼96 Ma (Rotstein et al., 1991), partially separating the William's Ridge-Broken Ridge system from the main Kerguelen Plateau (Munschy, Dyment, et al., 1992; Rotstein et al., 1991). The Labuan Basin extends farther southeast, bounding the northeastern edge of the SKP (Rotstein et al., 1991; Whittaker et al., 2013). Although similarities between the Labuan Basin and SKP can be found in the sedimentary record, the nature of the basement of the Labuan Basin is unknown (Rotstein et al., 1991). The conjugate margin of the Labuan Basin, the Diamantina Zone on the Australian plate, is elongated and has extremely rough basement topography, with basement comprising basalt, gabbro, and peridotite (Beslier et al., 2004; Cande & Mutter, 1982; Munschy, Dyment, et al., 1992). During the Australian-Antarctic rifting, the Diamantina Zone formed concurrently with the Labuan Basin, representing its former northeast extension (Beslier et al., 2004; Whittaker et al., 2013).

2.2. Deformation Migration Concept for Rifted Margins Classification

Archetypes of "magma-poor" and "magma-rich" continental rifted margins are the Atlantic end members: the magma-poor Iberia-Newfoundland and the magma-rich mid-Norway-East Greenland conjugate pairs. Although each conjugate pair differs in terms of magmatic imprint, tectonic structure, and sedimentary thicknesses and compositions, first-order structural similarities can be observed (Peron-Pinvidic et al., 2013). The resulting across-strike division into "domains" and related nomenclature (Peron-Pinvidic et al., 2013) have been adopted for the classification of other continental rift systems such as Angola-Brazil (Peron-Pinvidic et al., 2013), the South China Sea (Franke et al., 2014), Bay of Biscay-Pyrenees (Tugend et al., 2014), Gulf of Aden (Chenin et al., 2022), and Alpine Tethys (Chenin et al., 2022). The structural domains that characterize the rifted margins deformation migration model progress, younger and oceanward, from proximal to necking, distal, outer, and ultimately oceanic (Peron-Pinvidic et al., 2013). The proximal domain is typically formed by moderately extended continental crust, with distinctive horsts and grabens bounded by high-angle normal faults and containing wedge-shaped syn-tectonic sediment packages. The necking domain reflects extreme extension and deformation/coupling between the continental crust and the mantle lithosphere. Recent studies show how extreme extension may be controlled by long-offset crustal-scale detachment faults (Chao et al., 2021; Gresseth et al., 2023; Osmundsen & Péron-Pinvidic, 2018). The deformation/coupling is associated with an inflection of the Moho, corresponding to substantial crustal thinning and tilting, which leads to the formation of a wedge-shaped crustal domain (Peron-Pinvidic et al., 2013). The distal domain is characterized by low-angle normal faults and is typically an area of hyperextended crust. The outer domain represents the area potentially dominated by syn-rift magmatism and may encompass either the ocean continent transition or the continent-ocean boundary. The oceanic domain consists of purely oceanic crust (Peron-Pinvidic et al., 2013).

3. Methods

3.1. Multichannel Seismic Reflection (MCS)

In this study, we present MCS profiles from three voyages to William's Ridge and Broken Ridge (Figures 1 and 2): RV *Investigator* IN2020_V01 (2020) (Coffin et al., 2023c), RV *Sonne* SO272 (2020) (Uenzelmann-Neben, 2020, 2021a, 2021b), and RV *Rig Seismic* RS179 (1997) (Borissova et al., 2002). Data from RV *Investigator* and RV *Sonne* are presented here for the first time, whereas we reinterpret the RS179-07 profile, resulting in a better fit with our stratigraphic framework. Although the resolution of the data sets is similar in the upper stratigraphic sections, the longer streamers deployed during cruises SO272 and RS179 allowed the seismic patterns that characterize the deeper sections of the MCS profiles to be imaged with higher resolution compared to the IN2020_V01 data set. Processing and interpretation of the new IN2020_V01 and SO272 MCS profiles have been performed using GLOBE Claritas, IHS Kingdom and Paradigm software. A detailed explanation of acquisition parameters and processing methods of the MCS data sets analyzed in this study can be found in Supporting Information S1.

3.1.1. Correlation of Stratigraphic Horizons and Units

MCS data allow us to discern seismic units with similar patterns. Distinctive patterns and geometric relationships between reflections were used to interpret the main unconformities, which are horizons of erosion or no deposition. Seismic units and key unconformities, consistently interpreted on William's Ridge and the eastern part of Broken Ridge, were correlated with features bearing similar characteristics, imaged by several MCS and SCS profiles acquired on the central and northern CKP, SKP, and western Broken Ridge (Borissova et al., 2002; Coffin et al., 1990; Colwell et al., 1988; Driscoll et al., 1991; Houtz et al., 1977; Munschy & Schlich, 1987; Munschy, Fritsch, et al., 1992; Rotstein et al., 1992) (Figure 1, Table 1). Correlation with key horizons on the CKP, SKP, and Broken Ridge enables us to tentatively align our horizons with age dates from cores drilled at DSDP and ODP sites (Barron et al., 1989, 1991; Coffin et al., 2000, 2002; Davies et al., 1974; Frey et al., 2003; Peirce et al., 1989; Schlich et al., 1989; Weissel et al., 1991; Wise et al., 1992) (Figure 1, Table 1), to further refine the interpreted relative dating inferred from the seismic stratigraphy.

The locations of ODP Leg 120 Site 747 and Leg 119 Site 738 (Barron et al., 1989; Schlich et al., 1989) were crossed by MCS profiles acquired, respectively, on the central CKP (Munschy, Fritsch, et al., 1992) and SKP (Rotstein et al., 1992) (Figures 1 and 2; Table 1). On Broken Ridge, the location of ODP Leg 121 Sites 752, 754, and 755 (Peirce et al., 1989) were crossed by a SCS profile analyzed by Driscoll et al. (1991) (Figures 1

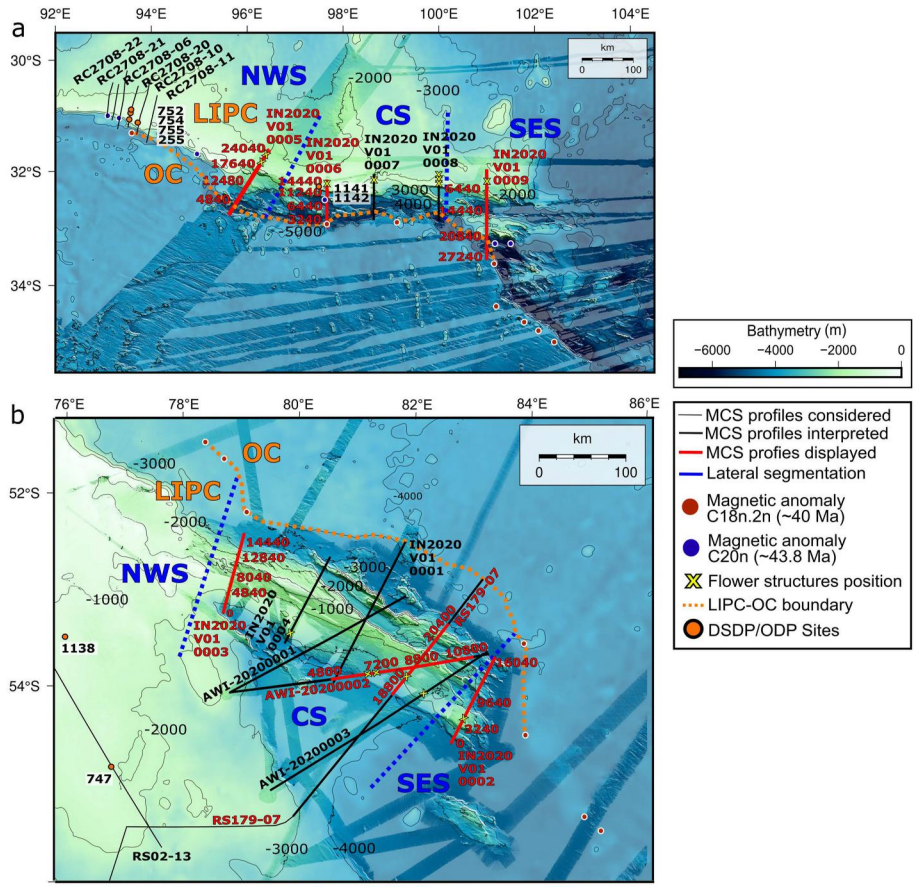

Figure 2. GEBCO, 2023 gridded bathymetric map (GEBCO, 2023) (transparent) and multibeam bathymetry of Broken Ridge (Coffin et al., 2023a; Picard et al., 2018) (a) and William's Ridge—Kerguelen Plateau (Beaman, 2023; Coffin et al., 2023b; Dreutter et al., 2020) (b). Location of the two study areas (William's Ridge and Broken Ridge) shown in red boxes in Figure 1. Thin black lines, thick black lines, and red lines represent MCS profiles, respectively, considered, interpreted, and shown in this study. Blue dotted lines mark the boundaries between different segments of the conjugate rifted margins. CS, central segment; LIPC, Large Igneous Province (LIP) crust (Kerguelen mantle plume related); NWS, northwest segment; OC, oceanic crust (normal seafloor spreading); SES, southeastern segment. Ages of magnetic anomalies are from Tikku and Cande (1999); Ségoufin et al. (2004).

and 2; Table 1). Drill site locations crossed by MCS and SCS profiles enabled accurate core-seismic correlations between unconformities and stratigraphic units, on each conjugate margin, in the geological and geophysical data. We build on these correlations and use them as a reference to further correlate and tie the MCS data set analyzed herein.

3.1.2. Tectonic Structures: Nomenclature

We use C18n.2n magnetic anomaly picks proposed by Ségoufin et al. (2004) to demarcate unequivocal oceanic crust, progressively emplaced by normal seafloor spreading at the SEIR, whereas uncertainties remain in delineating the transitional area between LIP crust, emplaced by the Kerguelen mantle plume, and oceanic crust (Figure 2).

We therefore demarcate one extent of the transitional zone with Chron C18n.2n (~40 Ma), which is the closest magnetic anomaly lineation to William's Ridge and Broken Ridge (Figure 2). We do not include C20n magnetic anomaly picks (Tikku & Cande, 1999) in our analysis that are inconsistent across conjugate end members (Figure 2).

In addition, the C20n pick interpreted by Tikku and Cande (1999) at profile IN2020_V01-006 (Figure 2) corresponds to a tectonic structure that we suggest is part of Broken Ridge, and therefore LIP crust, following the

Journal of Geophysical Research: Solid Earth

10.1029/2023JB027493

Table 1
Stratigraphic Framework of William's Ridge (Kerguelen Plateau) and Broken Ridge

(This study) seismic unit	(This study) upper boundary name	(This study) upper boundary age (Ma) [a]	(This study) temporal evolution	Lithology (DSDP-ODP sites[b])	Correlation (boundary)		Correlation (seismic unit)					
					WR[c]	KP[d]	Central CKP[e]	BR[f]	Northern CKP[g]	SKP[h]	SKP[i]	SKP[j]
Q1	wb	Present day	Post-rift	Foraminifer/diatom nannofossil ooze. Ice-rafted debris (Kerguelen)	wb-miou	Water-A-B (?)	Q1-NQ1-N2-N1	S-III	S1	A	NQ1	UPM
NQ1	miou	~5	Post-rift	Nannofossil ooze, occasional vitric ash	miou-olig	Water-A-B (?)	Q1-NQ1-N2-N1	S-III	S2	A	NQ1	UPM
PN1	miol	~23	Post-rift	Nannofossil ooze, occasional vitric ash	miou-olig	Water-A-B (?)	PN1	S-III	(?)	B	PN1	UPM
P2	olig	~34	Syn-rift	Calcareous nannofossil ooze, chalks, limestone, volcanic ash	olig-eoc	Water-A-B (?)	P	O-I–O-II	I1	C	P2	POM
P1	eoc	~44	Syn-rift	Calcareous nannofossil ooze, chalks, limestone, volcanic ash	eoc-camp	Water-A-B (?)	P	S-II	I1	D	P1	POM
K3	maas	~66	Pre-rift	Chalk, limestone, volcanic ash	camp-alb	A-B (?)	K	S-I	I2	E	K3	PRM
K1-2	camp	~83	Pre-rift	Chalk, limestone	alb-Lbbw	B-C (?)	K	S-I	I3	F	K1–K2	PRM
BC	Lbbw/ceno	~93–109/~98–99	Pre-rift	Basalt	Lbbw	Basement	Basement	/	/	Basement complex	BC	Basement

Note. BR, Broken Ridge; CKP, Central Kerguelen Plateau; KP, Kerguelen Plateau; SKP, Southern Kerguelen Plateau; WR, William's Ridge. [a]Walker and Geissman (2022). [b]Schlich et al. (1989), Peirce et al. (1989), Barron et al. (1989), and Frey et al. (2003). [c]Borissova et al. (2002). [d]Houtz et al. (1977). [e]Munschy, Fritsch, et al. (1992). [f]Driscoll et al. (1991). [g]Munschy and Schlich (1987). [h]Colwell et al. (1988). [i]Coffin et al. (1990). [j]Rotstein et al. (1992).

interpretation of Driscoll et al. (1991). This across-strike segmentation is the foundation on which we build the classification of structural entities of the William's Ridge-Broken Ridge rifted margins, following the nomenclature proposed by Peron-Pinvidic et al. (2013).

Based on the morphology of the tectonic features observed on the MCS profiles, we divide the William's Ridge-Broken Ridge conjugate pair into three along-strike segments, northwest (NWS), central (CS), and southeast (SES) (Figures 1 and 2). The NWS includes the northern CKP and the western part of Broken Ridge (Figures 1 and 2). The CS encompasses the central CKP and the eastern part of BR (Figures 1 and 2). The SES extends to the western part of Labuan Basin-Diamantina Zone (Figures 1 and 2).

3.2. Bathymetry

In this study, we consider four different bathymetric grids for the analysis of seafloor structures (Figures 1 and 2). We integrate multibeam bathymetry collected on several voyages to Kerguelen Plateau and Broken Ridge (Beaman, 2023; Coffin et al., 2023a; Picard et al., 2018) with GEBCO-2023 gridded bathymetry (GEBCO, 2023) (Figures 1 and 2). We use the bathymetric data set for validation of the shape, lateral extent, and depth of tectonic features imaged by the MCS data. In addition, we have determined the true dip angles of the normal faults outcropping on the seafloor in the NWS, CS, and SES by using bathymetric profiles, in the approximate locations of the MCS transects, perpendicularly to the strikes, the rift shoulder, the tilted blocks, and the rotated blocks.

3.3. Plate Tectonic Reconstruction

GEBCO-2023 gridded bathymetry (GEBCO, 2023), and the new and legacy MCS profiles were reconstructed to Late Cretaceous and Paleogene time slices using GPlates 2.2.0 software (Boyden et al., 2011) and the plate model of Whittaker et al. (2013). The Kerguelen mantle plume is reconstructed using the O'Neill et al. (2005) moving hotspot reference frame. However, we note that there is uncertainty regarding the paleo-location of the Kerguelen mantle plume (e.g., Müller et al., 1993; Steinberger & O'Connell, 1998; O'Neill et al., 2005; Doubrovine et al., 2012), and even pinpointing an exact current location for the Kerguelen hotspot is uncertain with studies showing Neogene volcanism occurring on active Heard Island, in the Kerguelen Islands (Bénard et al., 2010), and on Shell Bank (Duncan et al., 2016).

4. Stratigraphic Framework of Kerguelen Plateau-Broken Ridge

Numerous legacy MCS and SCS profiles across the Kerguelen Plateau and Broken Ridge have previously been acquired and interpreted (Borissova et al., 2002; Coffin et al., 1990; Colwell et al., 1988; Driscoll et al., 1991; Houtz et al., 1977; Munschy & Schlich, 1987; Munschy, Fritsch, et al., 1992; Rotstein et al., 1992). Several independent terminologies, related to the recognized seismic and lithologic units, were adopted in each study. Furthermore, no consistent interpretation across the Kerguelen Plateau and Broken Ridge is published. For the Kerguelen Plateau, two studies propose a unified naming scheme for each seismic unit and horizon; Munschy, Fritsch, et al. (1992) adopted the nomenclature used by Coffin et al. (1990), and Borissova et al. (2002) who focused on correlations between unconformities at the bottom of each seismic unit (Table 1). Here, we correlate unconformities and seismic units across both the Kerguelen Plateau and Broken Ridge for the first time, suggesting a division into pre-, syn-, and post-rift units recognized in newly acquired as well as legacy MCS and SCS data, and DSDP and ODP sites.

We follow the nomenclature proposed by Borissova et al. (2002) for unconformities and the terminology implemented by Coffin et al. (1990) and Munschy, Fritsch, et al. (1992) for sedimentary units. We define four sedimentary units, deposited above the igneous basement, along the strike of the William's Ridge-Broken Ridge conjugate rifted margins. The pre-rift foundation is characterized by the crystalline igneous "bas" and sedimentary units "K1-2" and "K3," whereas the syn-rift infill is represented by seismic units "P1" and "P2." Within the pre- and syn-rift seismic units we identify five unconformities: "Lbbw" (~93–109 Ma)/"ceno" (~98–99 Ma), "camp" (~83 Ma), "maas" (~66 Ma), "eoc" (~44 Ma), and "olig" (~34 Ma). The "olig" unconformity represents a long-lasting uplift of the rift flank of ~10 Ma, after the onset of seafloor spreading, similarly to what has been proposed for the magma-poor rifted margins case of SW Florida (Pindell et al., 2014) We refer here to post-rift seismic units as the sedimentary units deposited above horizon "olig." However, we do not interpret this package in further detail as it is subject of an ongoing complementary study.

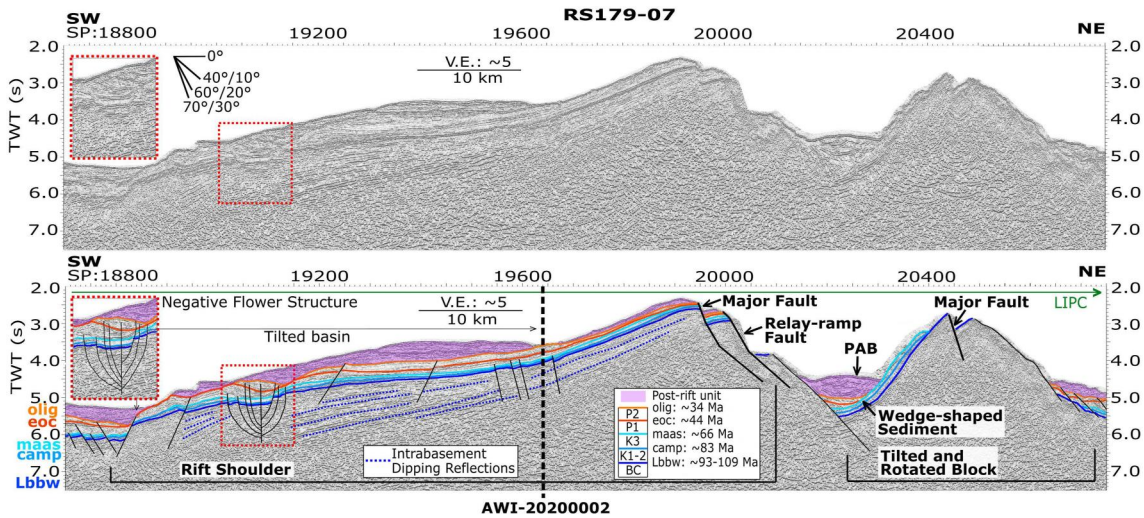

Figure 3. *RV Rig Seismic* MCS profile RS179-07 across William's Ridge (Borissova et al., 2002). Uninterpreted (top) and interpreted (bottom) seismic showing the main unconformities (solid colored lines) and faults (black lines). Blue lines represent pre-rift unconformities; orange lines indicate syn-rift unconformities. See Table 1 for key to seismic units and boundaries. Red dotted box includes a characteristic negative flower structure within the seismic sequences. Black dotted line: intersection with MCS profile AWI-20200002. LIPC, Large Igneous Province (LIP) crust; PAB, pull-apart basin. Vertical exaggeration: ~5. Angles displayed in the upper panel show vertically exaggerated values on the left, and true-to-scale values on the right.

For our area of focus, William's Ridge and eastern Broken Ridge, we adopt the ~93–109 Ma range of ages for CKP igneous basement, derived from crystallization ages calculated from $^{40}Ar/^{39}Ar$ incremental heating experiments on basalt samples cored at ODP Leg 183 Site 1138 (Figure 1) (Jiang et al., 2021). For eastern Broken Ridge we adopt the range of ages of ~98–99 Ma, derived from crystallization ages calculated from $^{40}Ar/^{39}Ar$ incremental heating experiments on basalt samples cored at Leg 183 Sites 1141–1142 (Jiang et al., 2021) (Figure 1). Control on ages of horizons and compositions of the sedimentary units comes from ODP Sites 738 and 747 on the Kerguelen Plateau, and DSDP Leg 26 Site 255, ODP Sites 752, 754, and 755 on Broken Ridge (Barron et al., 1989, 1991; Coffin et al., 2000; Davies et al., 1974; Frey et al., 2003; Peirce et al., 1989; Schlich et al., 1989; Weissel et al., 1991; Wise et al., 1992) (Figure 1). On the Kerguelen Plateau, the Paleogene and late Cretaceous sedimentary sequences at ODP Site 738 are biostratigraphically dated by calcareous nannofossils and planktonic foraminifera (Barron et al., 1989; Berggren, Kent, Flynn, & Van Couvering, 1985), whereas at ODP Site 747 biostratigraphy is referenced to paleomagnetic data (Berggren, Kent, & Flynn, 1985; Berggren, Kent, Flynn, & Van Couvering, 1985; Berggren, Kent, & Van Couvering, 1985; Schlich et al., 1989). The same approach of combining biostratigraphy and magnetostratigraphy is adopted for the analysis of ODP Sites 752, 754, and 755 cores on Broken Ridge (Berggren, Kent, Flynn, & Van Couvering, 1985; Peirce et al., 1989), whereas biostratigraphy was undertaken on DSDP Site 255 cores (Davies et al., 1974).

4.1. Pre-Rift Foundation

4.1.1. Igneous Basement: BC—Lbbw/Ceno

On the MCS data, the igneous basement "BC" is characterized by scattered or near parallel reflections (Figures 3–9; Figures S2–S7 in Supporting Information S1). On WR we identify intra-basement dipping reflections characterized by wedge shapes, and truncations at the sediment-basement interface. Their total thickness is at least 1 s (TWT) and they can extend for more than 20 km laterally (Figures 3 and 7; Figures S2 and S3 in Supporting Information S1). On Broken Ridge we do not identify any intra-basement dipping reflections, possibly due to the difference in resolution of deeper sections, compared to the William's Ridge data set.

MSC data enable the identification of the deepest major unconformity to be the top basement unconformity "Lbbw" or "ceno," whether located on William's Ridge or Broken Ridge, respectively (Figures 3–9; Figures S2–S7 in Supporting Information S1). Intersections of legacy MCS profile 179-07 (Borissova et al., 2002) and new profiles AWI-20200001, AWI-20200002, AWI-20200003, and IN2020_V01-0001 (Figure 7; Figures S2, S3, and S7 in Supporting Information S1) enabled direct correlation of the "Lbbw" seismic horizon. We further correlate

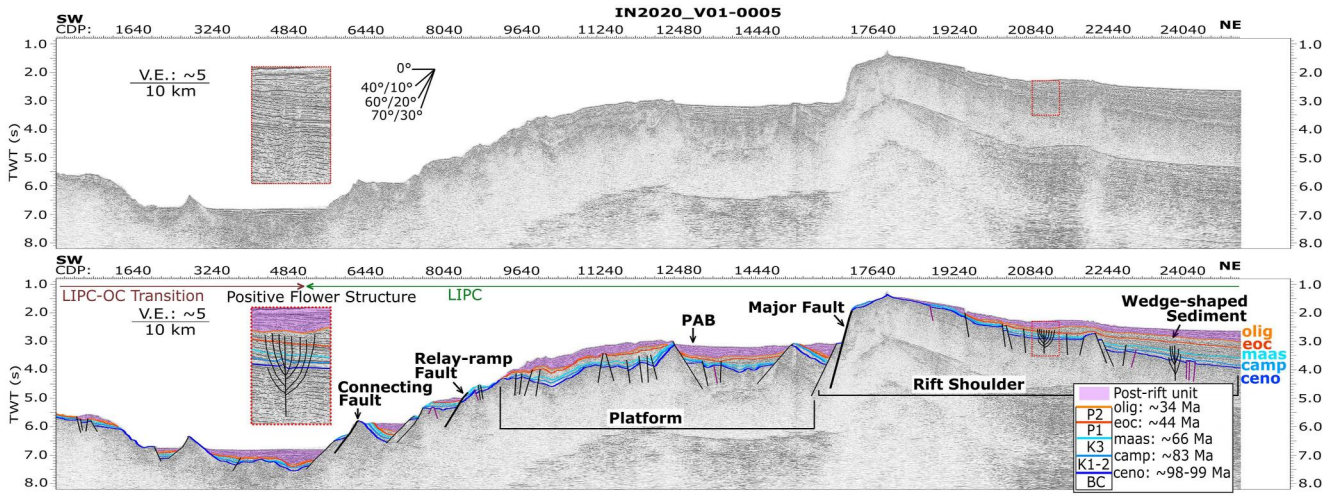

Figure 4. *RV Investigator* MCS profile IN2020_V01-0005 across Broken Ridge. Uninterpreted (top) and interpreted (bottom) seismic showing the main unconformities (solid colored lines), pre-rift faults (dark purple lines) and syn-rift faults (black lines). Blue lines represent pre-rift unconformities; orange lines indicate syn-rift unconformities. See Table 1 for key to seismic units and boundaries. Red dotted box shows a characteristic positive flower structure within the seismic sequences. LIPC, Large Igneous Province (LIP) crust; OC, oceanic crust; PAB, pull-apart basin. Vertical exaggeration: ~5. Angles displayed in the upper panel show vertically exaggerated values on the left, and true-to scale-values on the right.

the surface with unconformities on the northern and southern CKP (Munschy, Fritsch, et al., 1992; Munschy & Schlich, 1987), and the SKP (Barron et al., 1989; Coffin et al., 1990; Colwell et al., 1988; Rotstein et al., 1992) (Table 1). On Broken Ridge, we correlate the "ceno" horizon with the bottom boundary of sequence S-I (Driscoll et al., 1991) and unit IIC-IIB at ODP Site 755 (Peirce et al., 1989), assuming a similar age of ~98–99 Ma for the basement complex as basalts cored at ODP Sites 1141–1142 (Figure 1) (Jiang et al., 2021).

4.1.2. Sedimentary Units: K1-2—Camp and K3—Maas

Stratigraphically above "bas," units K1-2 and K3 have similar characteristics on both conjugate rifted margins, showing occasional near parallel and semi-continuous reflections (Figures 3–9; Figures S2–S7 in Supporting Information S1). We first correlate the seismic units with consistent patterns interpreted on MCS profiles on the southern CKP (Munschy, Fritsch, et al., 1992) and SCS profiles on western Broken Ridge (Driscoll et al., 1991).

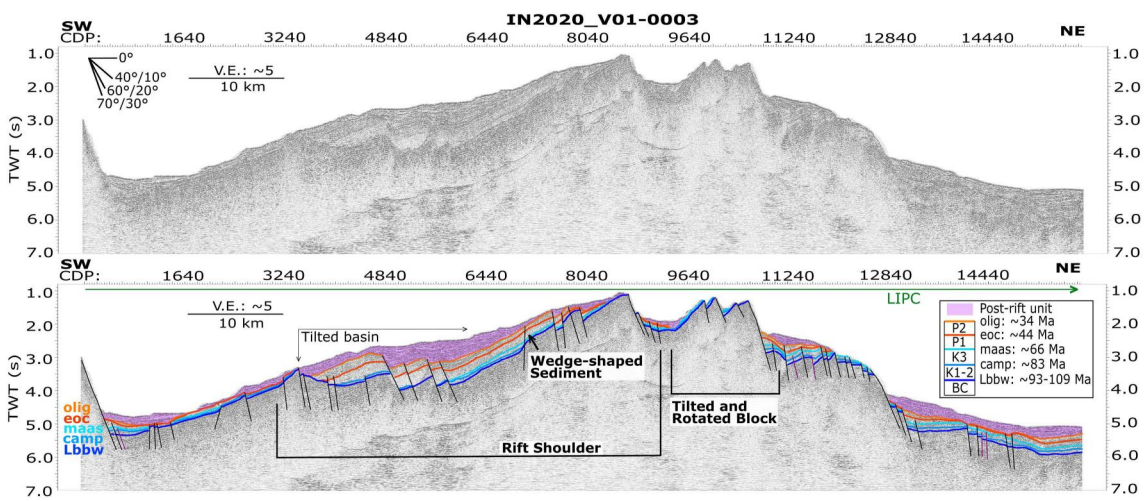

Figure 5. *RV Investigator* MCS profile IN2020_V01-0003 across William's Ridge. Uninterpreted (top) and interpreted (bottom) seismic showing the main unconformities (solid colored lines), pre-rift faults (dark purple lines) and syn-rift faults (black lines). Blue lines represent pre-rift unconformities; orange lines indicate syn-rift unconformities. See Table 1 for key to seismic units and boundaries. LIPC, Large Igneous Province (LIP) crust. Vertical exaggeration: ~5. Angles displayed in the upper panel show vertically exaggerated values on the left, and true-to-scale values on the right.

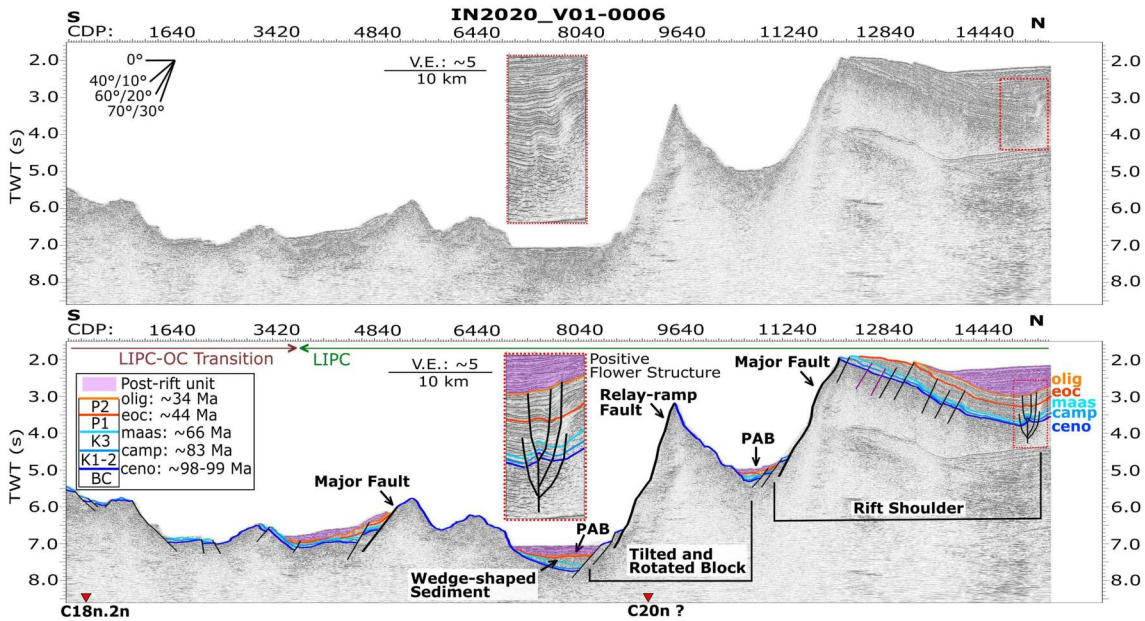

Figure 6. *RV Investigator* MCS profile IN2020_V01-0006 across Broken Ridge. Uninterpreted (top) and interpreted (bottom) seismic showing the main unconformities (solid colored lines), pre-rift faults (dark purple lines) and syn-rift faults (black lines). Blue lines represent pre-rift unconformities; orange lines indicate syn-rift unconformities. See Table 1 for key to seismic units and boundaries. Red dotted box shows a characteristic positive flower structures within the seismic sequences. LIPC, Large Igneous Province (LIP) crust; OC, oceanic crust; PAB, pull-apart basin. Vertical exaggeration: ~5. Angles displayed in the upper panel show vertically exaggerated values on the left, and true-to-scale values on the right.

We further extend our correlation with seismic units I3 and I2 (Munschy & Schlich, 1987) on the northern CKP, and to seismic units F-E (Colwell et al., 1988), K1-K2-K3 (Coffin et al., 1990), and PRM (Rotstein et al., 1992) on the SKP (Table 1). The composition of sequences K1-2 and K3 is predominantly chalks and limestones, with the presence of volcanoclastic material and volcanic ash in the upper part of K3 (Peirce et al., 1989; Schlich et al., 1989) (Figures 1 and 3).

The upper boundaries of carbonate sequences K1-2 and K3 are, respectively, continuous and discontinuous reflections "camp" and "maas" (Figures 3–9; Figures S2–S7 in Supporting Information S1). The unconformity we here name "camp" has been similarly observed in a previous interpretation of MCS profile 179-07 on William's Ridge (Borissova et al., 2002) (Figures 1–3). To be consistent with correlations between seismic patterns

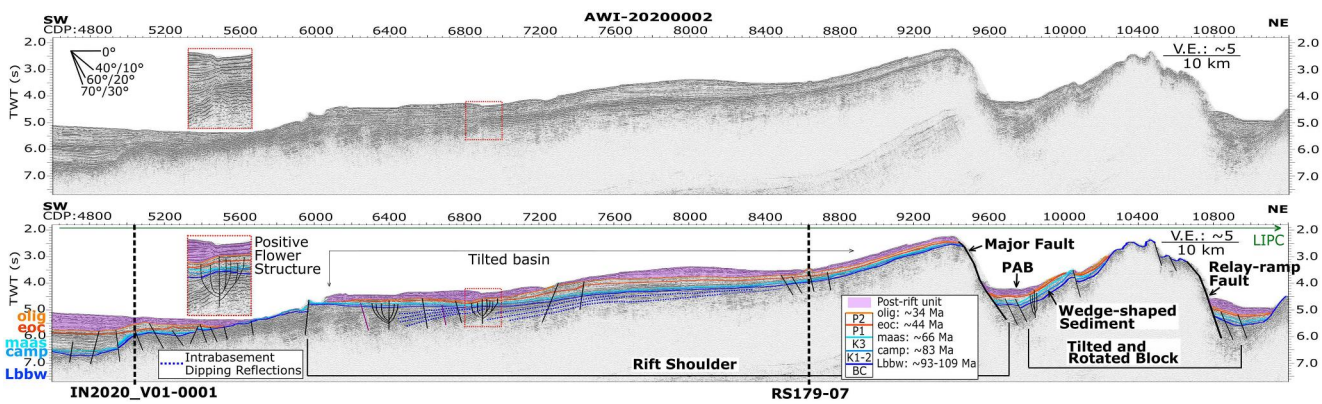

Figure 7. *RV Sonne* MCS profile AWI-20200002 across William's Ridge. Uninterpreted (top) and interpreted (bottom) seismic showing the main unconformities (solid colored lines), pre-rift faults (dark purple lines) and syn-rift faults (black lines). Blue lines represent pre-rift unconformities; orange lines indicate syn-rift unconformities. See Table 1 for key to seismic units and boundaries. Red dotted box shows a characteristic positive flower structure within the seismic sequences. Black dotted lines: intersection with MCS profiles IN2020_V01-0001 and RS179-07. LIPC, Large Igneous Province (LIP) crust; PAB, pull-apart basin. Vertical exaggeration: ~5. Angles displayed in the upper panel show vertically exaggerated values on the left, and true-to-scale values on the right.

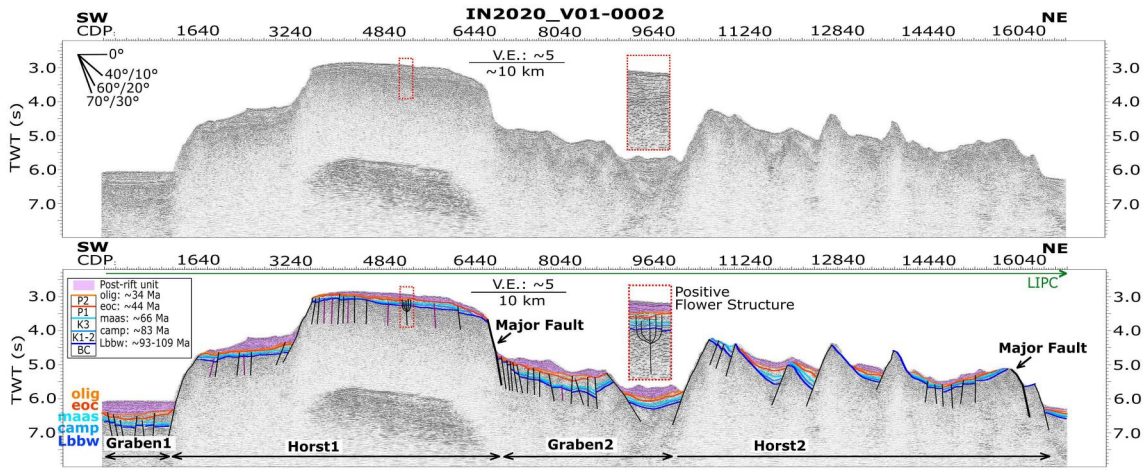

Figure 8. *RV Investigator* MCS profile IN2020_V01-0002 across William's Ridge. Uninterpreted seismic at the top and interpreted seismic showing the main unconformities (solid colored lines), pre-rift faults (dark purple lines) and syn-rift faults (black lines) at the bottom. Blue lines represent pre-rift unconformities; orange lines indicate syn-rift unconformities. See Table 1 for key to seismic units and boundaries. Red dotted box shows a characteristic positive flower structures within the seismic sequences. LIPC, Large Igneous Province (LIP) crust. Vertical exaggeration: ~5. Angles displayed in the upper panel show vertically exaggerated values on the left, and true-to-scale values on the right.

interpreted to this point, we suggest "camp" nomenclature to represent the bottom Campanian unconformity that Borissova et al. (2002) proposed to be nearly top Albian. We correlate the "camp" horizon with unconformities interpreted on MCS profiles on the CKP (Munschy & Schlich, 1987; Munschy, Fritsch, et al., 1992; Schlich et al., 1989) and SKP (Coffin et al., 1990). Rotstein et al. (1992) correlated horizons imaged on MCS data acquired on the SKP to the interpretation proposed by Coffin et al. (1990) and further tied the seismic profiles with ODP Site 738 (Barron et al., 1989), where a consistent unconformity of Campanian age was observed (Figure 1, Table 1). Although we recognize a distinct unconformity that we interpret as "camp" in the Broken Ridge dataset, correlation with published data is less robust than for Kerguelen. No unconformities bearing similar ages were recognized on SCS profiles (Driscoll et al., 1991) and we can therefore only correlate the horizon with the top boundary of unit IIA at ODP Site 755 (Peirce et al., 1989) (Table 1).

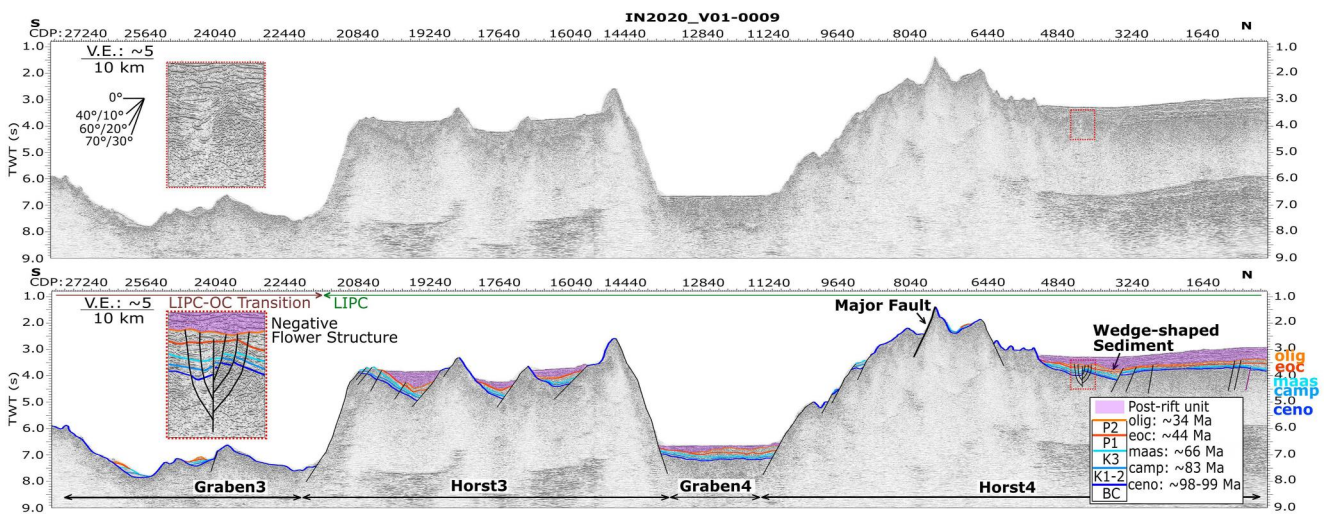

Figure 9. *RV Investigator* MCS profile IN2020_V01-0009 across Broken Ridge. Uninterpreted (top) and interpreted (bottom) seismic showing the main unconformities (solid colored lines), pre-rift faults (dark purple lines) and syn-rift faults (black lines). Blue lines represent pre-rift unconformities; orange lines indicate syn-rift unconformities. See Table 1 for key to seismic units and boundaries. Red dotted box shows a characteristic negative flower structure within the seismic sequences. LIPC, Large Igneous Province (LIP) crust; OC, oceanic crust. Vertical exaggeration: ~5. Angles displayed in the upper panel show vertically exaggerated values on the left, and true-to-scale values on the right.

The "maas" terminology is applied to the prominent top Maastrichtian unconformity observed above the horizon "camp" and unit K3. Building on the stratigraphic framework proposed so far, we suggest that horizon "maas" corresponds to a similar unconformity termed "camp" in the previous interpretation of MCS profile RS179-07 on William's Ridge (Borissova et al., 2002). Although not recognized previously on William's Ridge (Borissova et al., 2002), the "maas" unconformity is consistently observed on the CKP and western Broken Ridge. To estimate a relative age, we first correlate the horizon with the unconformity recognized nearby, on the central CKP (Munschy, Fritsch, et al., 1992; Schlich et al., 1989), and on western Broken Ridge (Driscoll et al., 1991; Peirce et al., 1989) (Figures 1 and 3). On the central CKP, the correlation is with the boundary between seismic units K and P (Munschy, Fritsch, et al., 1992), and units III and IIC (Schlich et al., 1989), whereas on western Broken Ridge with the boundary between seismic units S-I and S-II (Driscoll et al., 1991), the bottom boundary of unit IIC at ODP Site 752, and top boundary of unit II at ODP Site 754 (Peirce et al., 1989) (Figure 1, Table 1). We further extend our correlation with MCS data and ODP Site 738 on the SKP (Barron et al., 1989; Coffin et al., 1990; Colwell et al., 1988; Rotstein et al., 1992) (Table 1).

4.2. Syn-Rift Infill

4.2.1. Sedimentary Units: P1—Eoc and P2—Olig

On northwestern William's Ridge, seismic units P1 and P2 are chaotic, occasionally characterized by scattered reflections (Figures 3, 5, and 7; Figures S2, S3, S5, and S7 in Supporting Information S1). Moving southeast, seismic units P1 and P2 assume near parallel reflections and a less chaotic pattern (Figure 9). On eastern Broken Ridge, seismic units P1 and P2 are typically characterized by parallel, and stratified reflections (Figures 4, 6, and 9; Figures S4 and S6 in Supporting Information S1). Although the seismic pattern we observe on northwestern William's Ridge does not have any analogs on the CKP, a chaotic internal structure has been observed in seismic unit O-I on western Broken Ridge (Driscoll et al., 1991). Most seismic patterns observed on William's Ridge and eastern Broken Ridge are used for further correlations. We first correlate sequences P1 and P2 with similar seismic patterns observed in sequence P (Munschy, Fritsch, et al., 1992) on the central CKP, and O-II and S-II (Driscoll et al., 1991) on Broken Ridge. We then extend correlations to seismic unit I1 (Munschy & Schlich, 1987) on the northern CKP, and with sequences D-C (Colwell et al., 1988), P1-P2 (Coffin et al., 1990), and POM (Rotstein et al., 1992), on the SKP (Table 1). We propose the composition of units P1 and P2 on William's Ridge to be a combination of erosional material from K3, calcareous nannofossil ooze, and micritic chalk (Coffin et al., 2000; Peirce et al., 1989; Schlich et al., 1989).

The laterally discontinuous erosional unconformity "eoc" (Figures 3–9; Figures S2–S7 in Supporting Information S1) separates seismic units P1 and P2 (Figures 3–9; Figures S2–S7 in Supporting Information S1). The same horizon we term "eoc" has been previously recognized and given the same interpreted relative age of ∼44 Ma on WR (Borissova et al., 2002). Unconformity "eoc" is well controlled as it is observed in other areas of the CKP and western Broken Ridge. This unconformity correlates with hiatuses of a duration of ∼21 Ma (∼23? to ∼44 Ma) (Munschy & Schlich, 1987) and ∼14 Ma (∼38–∼52 Ma) (Schlich et al., 1989) prevalent on the CKP (Table 1). The ages of the hiatuses recognized on the southern and northern CKP are based, respectively, on ODP Site 747 (Munschy, Fritsch, et al., 1992) and piston core EL54-7 (Markl, 1973; Munschy & Schlich, 1987). On Broken Ridge, the "eoc" unconformity correlates to the unconformity separating onlapping seismic units O-I and O-II (Driscoll et al., 1991) (Table 1).

The prominent unconformity "olig" bounds the top of seismic unit P2 (Figures 3–9; Figures S2–S7 in Supporting Information S1). We consistently pick the same unconformity and suggest the same relative age as previously proposed in the interpretation of MCS profile RS179-07 on William's Ridge (Borissova et al., 2002). This unconformity can be correlated to the hiatuses observed on the northern CKP and SKP (Barron et al., 1989; Munschy & Schlich, 1987; Rotstein et al., 1992). On western Broken Ridge, we correlate the horizon with the boundary between an onlapping sequence (O-II) and a horizontal cap (S-III) (Driscoll et al., 1991) (Table 1). Further correlation with the "olig" unconformity can be extended to MCS profiles from the SKP (Barron et al., 1989; Borissova et al., 2002; Coffin et al., 1990; Colwell et al., 1988; Rotstein et al., 1992) (Table 1).

4.3. William's Ridge MCS Profile RS179-07: A New Interpretation

We propose a new interpretation of the legacy MCS profile RS179-07 (Borissova et al., 2002) (Figure 3) to align with our newly established seismo-stratigraphic framework. Within the igneous basement we consistently

identify dipping reflections. Furthermore, we recognize unconformity "Lbbw" (~93–109 Ma) is recognized to be the top basement reflection, and horizons "camp" (~83 Ma), "eoc" (~44 Ma), and "olig" (~34 Ma) (Borissova et al., 2002) in the overlying sedimentary sequences. In contrast, we do not identify the "alb" horizon, but instead interpret unconformity "maas" (Borissova et al., 2002) at ~66 Ma, which separates seismic unit K3, belonging to the pre-rift foundation, and seismic unit P1, part of the syn-rift infill. Therefore, our new interpretation of profile RS179-07 (Borissova et al., 2002) resolves the timing of the transition between pre-rift and syn-rift, in contrast to the previous interpretation suggesting a time window of ~40 Ma for the onset of rift uplift.

5. Tectonic Framework of William's Ridge-Broken Ridge

Legacy seismic profiles and satellite-derived free-air gravity data from the eastern Kerguelen Plateau have previously enabled morphological description of William's Ridge (Borissova et al., 2002; Coffin et al., 1986). On western Broken Ridge, structures imaged by SCS profiles were interpreted to explain its subsidence history (Driscoll et al., 1991). These interpretations are independent, and although they explain the tectonic evolution of each rifted margin, a thorough analysis of structures consistently found across the conjugate margins has not been undertaken previously. William's Ridge and eastern Broken Ridge are conjugates (Figures 1 and 2). In this study we analyze normal and transform faults characterizing the William's Ridge-eastern Broken Ridge margins. Given similar structural characteristics of both, we propose a unified classification in three segments, based on dominant fault patterns, including normal faults and flower structures.

5.1. The Northwest (NWS), Central (CS), and Southeast (SES) Segments

The NWS is represented by seismic line IN2020_V01-0005, acquired across Broken Ridge near the boundary with the CS (Figures 2 and 4). This profile images a predominant rift shoulder, with its shallowest depth at ~900 mbsl (~1.2 s TWT), which multibeam bathymetry shows progressively deepens toward the northeast (Figures 2 and 4). In addition, seismic line IN2020_V01-0005 shows an oceanward directed hanging block, which the bathymetry reveals to have a platform shape, ~50 km long (Figures 2 and 4). The rift shoulder is dissected by a low-angle normal fault, which displays a true dip of ~25° at the seafloor, based on the bathymetric data (Figures 2 and 4).

The CS on William's Ridge is the most densely surveyed area, as it has been imaged by both new and legacy MCS profiles (Figures 2, 3, 5, and 7; Figures S2, S3, S5, and S7 in Supporting Information S1). The profiles and multibeam bathymetry show a predominant rift shoulder, which is a prominent tilted block ~50 and ~85 km long, steadily and progressively deepening toward the southwest. Along the strike of William's Ridge's CS (Figure 2), the seafloor depth, at its shallowest on the rift shoulder, progressively increases from northwest (~750 mbsl; ~1 s TWT) to southeast (~2,100 mbsl; ~2.8 s TWT) (Figures 2, 3, 5, and 7; Figures S2, S3, S5, and S7 in Supporting Information S1). A tilted basin, defined by its boundaries being either downlapping geometries of "eoc" and "olig" onto pre-rift strata, or reflections cut by normal faults, is discernible along the entire strike of William's Ridge (Figures 2, 3, 5 and 7; Figures S2, S3, S5, and S7 in Supporting Information S1) On William's Ridge we consistently identify a tilted and rotated block located between the rift shoulder and the oceanic crust. The tilted and rotated block is ~10–20 km wide and its shallowest point is between ~750 and ~1,875 mbsl (~1 and ~2.5 s TWT; Figures 2, 3, 5 and 7; Figures S2, S3, S5, and S7 in Supporting Information S1). Analysis of bathymetric profiles in the William's Ridge CS shows that most low-angle normal faults dissecting the rift shoulder and the tilted and rotated block have true dips from ~26° to ~30° (Figures 2 and 5; Figures S2, S3, S5, and S7 in Supporting Information S1).

The CS imaged on bathymetric and MCS data on Broken Ridge shows, similarly to William's Ridge, a rift shoulder as a prominent tilted block, at least ~40 km long and consistently dipping to the north (Figures 2 and 6; Figures S4 and S6 in Supporting Information S1). Along the strike of Broken Ridge's CS (Figure 2) the shallowest point on the rift shoulder progressively deepens from west (~1,275 mbsl; ~1.7 s TWT) to east (~1,500 mbsl; ~2 s TWT) (Figures 2 and 6; Figures S4 and S6 in Supporting Information S1).

Compared to William's Ridge, the Broken Ridge rift shoulder is highly dissected by normal faults, dipping toward the north and south (Figure 6; Figures S4 and S6 in Supporting Information S1). However, on MCS profile IN2020_V01-0007 we observe horsts and grabens within the rift shoulder (Figure 2; Figure S6 in Supporting Information S1). Generally, the CS also displays a tilted and rotated block, ~10 km long, located between the Broken Ridge rift shoulder and oceanic crust (Figures 2 and 6; Figure S4 in Supporting Information S1), except

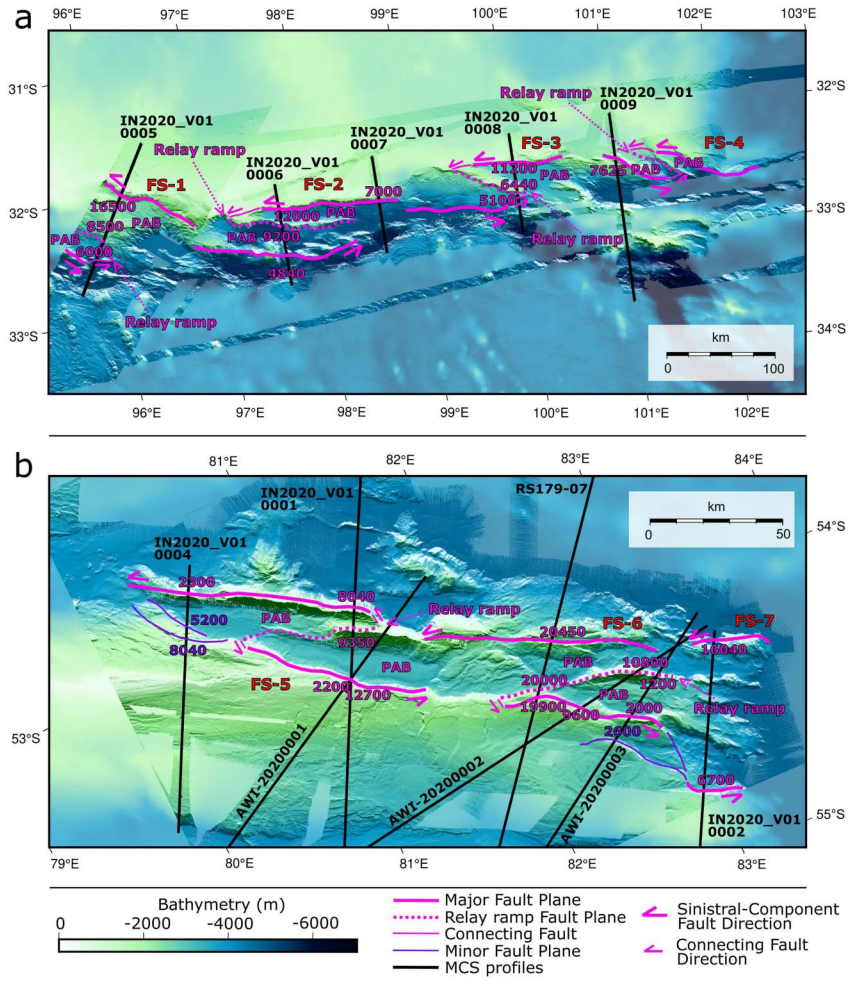

Figure 10. GEBCO, 2023 gridded bathymetric map (GEBCO, 2023) (transparent) and multibeam bathymetry of Broken Ridge (Coffin et al., 2023a; Picard et al., 2018) (a) and William's Ridge-Kerguelen Plateau (Beaman, 2023; Coffin et al., 2023b; Dreutter et al., 2020) (b). Solid black lines, MCS profiles; thick solid pink lines, major fault planes; thin sold pink lines, connecting faults; solid purple lines, minor fault planes; and thick dotted pink lines, relay ramp fault planes. FS, fault system; PAB, pull-apart basin.

for MCS section IN2020_V01-0007 (Figure 2; Figure S6 in Supporting Information S1). Instead, this profile shows, between the rift shoulder and the ocean crust, rough seafloor with outcropping pre-rift sequences. Bathymetric analysis shows the low-angle normal faults dissecting the rift shoulder, and the tilted and rotated block on the CS of Broken Ridge have true dips from ~25° to ~27° (Figures 2 and 6; Figures S4 and S6 in Supporting Information S1).

Bathymetric and MCS data acquired on the SES (Figures 1 and 2) of William's Ridge and Broken Ridge are characterized by horsts and grabens distributed symmetrically across the strike of both conjugate margins (Figures 2, 8, and 9). Profile IN2020_V01-0002 reveals two main horsts (Figures 2 and 8). Horst1 is roughly 30 km wide and its top lies in water depths of ~2,100 mbsl (~2.8 s TWT). Horst2 is heavily faulted, ~25 km wide, and ranges in depth from ~3,000 mbsl (~4 s TWT) to ~4,125 m (~5.5 s TWT). At the southwest end of this profile, we identify the sub-parallel Graben1. Between Horst1 and Horst2, a faulted tilted graben (Graben2 in Figure 8) has developed slightly dipping toward the northeast. In the southern part of profile IN2020_V01-0009, Horst3 is ~40 km long and its top is located at a depth of ~2,850 m (~3.8 s TWT) (Figures 2 and 9). In the northern part, Horst4 is at least ~60 km long and ranges in depth from ~1,125 (~1.5 s TWT) to ~2,100 (~2.8 s TWT) mbsl (Figures 2 and 9). The surface of this horst is smooth in the north and rough and eroded in the south. Between the horsts and the SEIR we recognize Graben3, characterized by an irregular surface representing widespread outcropping of igneous basement, and the planated Graben4, ~20 km long, located between Horsts3

and Horst4 (Figure 9). Bathymetric profiles show low angle normal faults of ∼27° on WR and ∼25° on Broken Ridge characterizing seafloor displacement between the main horsts and grabens (Figures 8 and 9).

5.2. Fault Systems and Flower Structures

Combined analysis of multibeam bathymetry (Beaman, 2023; Coffin et al., 2023a, 2023b; Dreutter et al., 2020; Picard et al., 2018) and MCS data enables 3D mapping of several fault systems, striking northwest-southeast on William's Ridge and Broken Ridge (Figures 3–10; Figures S2–S7 in Supporting Information S1). The fault systems encompass a pair of major faults, characterized by an extensional and sinistral component, and may include connecting faults, relay ramps, and pull-apart basins. On Broken Ridge, four fault systems (FS-1, FS-2, FS-3, FS-4) are present, where major fault conjugate pairs are connected through six connecting faults, a relay ramp, and two pull-apart basins (Figures 4, 6, 9, and 10a; Figures S4 and S6 in Supporting Information S1). On William's Ridge three fault systems (FS-5, FS-6, FS-7) are evident (Figures 3, 7, 8, and 10b; Figures S2, S3, S5, and S7 in Supporting Information S1). FS-5 and FS-6 are connected through three connecting faults, and a relay ramp which bounds two pull-apart basins. The conjugate pair of major faults in FS-7 is divided by several faults dipping in different directions (Figure 10b; Figures S2, S3, and S5 in Supporting Information S1). On William's Ridge, we further identify minor normal faults localized in the northwesternmost and southeasternmost portions. We define minor faults to weakness surfaces able to accommodate only a minor portion of the dominant stresses regulating the total amount of displacement.

Other types of faults recognized in the MCS profiles are flower structures. They appear below the top basement unconformity and cut the sedimentary units, until reaching horizon “olig” (Figures 3–9; Figures S2–S7 in Supporting Information S1). Within the Broken Ridge rift shoulder, a total of six positive flower structures are imaged by MCS profiles IN2020_V01-0005, IN2020_V01-0006 and IN2020_V01-0008, whereas two negative flower structures are displayed in MCS sections IN2020_V01-0007 and IN2020_V01-0009 (Figures 2, 4, 6, and 9; Figures S4 and S6 in Supporting Information S1). Within the William's Ridge rift shoulder, a total of four positive flower structures are present, imaged on MCS profiles AWI-20220002, IN2020_V01-0002, IN2020_V01-0004, and two negative flower structures displayed in RS179-07 and AWI-20220003 (Figures 2, 3, and 8; Figures S5 and S7 in Supporting Information S1).

6. Interpretation

6.1. Basement Complex Characteristics

In line with the interpretations of MCS data on Elan Bank (Borissova et al., 2003), and the Raggatt Basin and CKP (Borissova et al., 2002; Coffin et al., 1990; Colwell et al., 1988; Schaming & Rotstein, 1990; Schlich et al., 1993), we observe dipping reflections within the basement of William's Ridge (dotted blue lines Figures 3 and 7; Figures S2 and S3 in Supporting Information S1). These intra-basement dipping reflections are analogous to those interpreted in legacy MCS lines due to similar geometries such as wedge shape, and truncated at the sediment-basement interface. Intra-basement dipping reflections have previously been interpreted as either stratigraphic layering in continental crust or lava intercalated with volcaniclastic sediments (Colwell et al., 1988). Coffin et al. (1990) proposed the dipping reflections to represent lava flows (Schaming & Rotstein, 1990), comparable to features observed at the Rockall Plateau (Roberts, 1975) and Vøring Plateau (Eldholm et al., 1989). Legacy SCS profiles on Broken Ridge imaged a strong dipping reflection representing the potential top basement unconformity (Driscoll et al., 1991), which has been correlated to the oldest age (∼93 Ma) obtained at ODP Site 755 (Peirce et al., 1989) (Table 1). However, the attempt of drilling rocks below the dipping and truncated sequence (Driscoll et al., 1991) (S-I in Table 1) did not recover any rocks to relate to the potential igneous basement. In contrast, igneous basement basalts recovered at ODP Sites 1141 and 1142, have been interpreted as consistent with subaerial pyroclastic and lava flows emplaced at ODP Site 1138 on the Kerguelen Plateau (Coffin et al., 2000; Jiang et al., 2021) (Figure 1). Thus, on both the William's Ridge and Broken Ridge conjugate margins, we interpret dipping reflectors as dominantly lava flows, probably emplaced subaerially.

6.2. Sedimentary Sequences and Structural Evolution

We associate the formation of the “camp” unconformity, with the onset of seafloor spreading between Australia and Antarctica at ∼83 Ma (Cande & Mutter, 1982; Espurt et al., 2012; Sauermilch et al., 2019). The stratigraphic marker recording this major tectonic event is consistently found at a larger scale, on MCS profiles that cross the

entire length of the breakup boundary between Australia and Antarctica (Close et al., 2009; Direen et al., 2011; Leitchenkov et al., 2014; Sauermilch et al., 2019; Stagg et al., 2004; Totterdell et al., 2000). This age is based on the identification of magnetic anomalies in the oceanic crust between Australia and Antarctica (Cande & Mutter, 1982). In addition, the sedimentary record of marine ingression (Cande & Mutter, 1982) and dating of foraminifera biozonations (Totterdell et al., 2000) constitute evidence for the latest opening of the new Australian-Antarctic Basin in the Early Campanian.

The "maas" angular unconformity records the onset of uplift at ~66 Ma (Munschy, Fritsch, et al., 1992; Schlich et al., 1989). This horizon can be compared to the rift onset unconformity proposed by Falvey (1974). Although our MCS data set displays a sediment-starved system and therefore only allows us to infer the timing of rift shoulder and horst formation, rift onset uplift likely controlled their development through generation or reactivation of major normal faults (Munschy & Schlich, 1987; Peirce et al., 1989). In the rift shoulder case, the initially dominant normal faults have been interpreted as dissecting a relatively small tilted block on both end members (Munschy & Schlich, 1987; Peirce et al., 1989). In our MCS data set, the absence of syn-rift sedimentary sections overlying the pre-rift section of the tilted block may be related to the pre-rift sedimentary section dipping at higher angles than sedimentary sections on the rift shoulder. As a result, syn-rift sediment possibly slid onto the shallowest surface of the pre-rift tilted block and left it exposed. During their development, rift shoulders and horsts have experienced major deformation, expressed by internal normal faults (Figures 3–9; Figures S2–S7 in Supporting Information S1). In places, displacement of different parts of the rift shoulder led to the formation of internal tilted grabens, which consequently accommodated syn-rift sediment infill (Figures 3–9; Figures S2–S7 in Supporting Information S1). Tilted and rotated blocks are either absent or irregularly narrow (Driscoll et al., 1991; Munschy & Schlich, 1987) or wide platform shapes (Figure 5).

Horizon "eoc" corresponds to the ~44 Ma breakup unconformity (Falvey, 1974) between William's Ridge and Broken Ridge. A hiatus identified across the Central CKP between ~52 and ~38 Ma is thought to represent a time interval of continuous erosion due to vertical motion and breakup processes (Munschy, Fritsch, et al., 1992; Schlich et al., 1989). On Broken Ridge, the unconformity identified at ~47–50 Ma is thought to record the same tectonic event (Driscoll et al., 1991). This vertical motion recorded on both rifted end members can be partially related to the change in direction of relative Australian-Antarctic plate motions at ~50 Ma (Whittaker et al., 2013) The "olig" unconformity represent the marker of an enduring uplift stage after the onset of seafloor spreading, preceding the exclusive post-rift pelagic deposition (Pindell et al., 2014). On William's Ridge, the "olig" unconformity might also correlate with a major drop in sea level (e.g., Miller et al., 2020) and initiation of the Antarctic Circumpolar Current (e.g., Kennett, 1977) that were contemporaneous with the onset of major continental glaciation in Antarctica.

6.3. Syn-Rift Transform Motion

Relay ramps are reorientated bedding areas which form due to overstepping between normal faults or strike-slip faults, in extensional or transform systems, respectively (Larsen, 1988; Peacock & Sanderson, 1995). Typically, two separate faults propagate toward each other until they interact through the creation of a dipping area which facilitates the accommodation of vertical or horizontal stresses (Peacock & Sanderson, 1995). In transform systems, pull-apart basins have commonly been interpreted to form due to the separation of crustal material, driven by a segment of a strike-slip fault moving obliquely with respect to the direction of the master faults, in an area of tension (Burchfiel & Stewart, 1966; Mann et al., 1983). The combination of sinistral transform and extensional motion between Australia and Antarctica during rifting (Whittaker et al., 2013) likely generated different groups of faults systems, developing several relay ramps, connecting faults, minor faults, and pull-apart basins that are recognizable on both William's Ridge and Broken Ridge (Figure 11).

We observe flower structures in our data set that corroborate previous interpretations by manifesting strike-slip faults (Cunningham & Mann, 2007; Harding, 1985; Huang & Liu, 2017). They typically form where blocks move parallel to each other and may involve convergence/transpression (restraining bends) or divergence/transtension (releasing bends) (Biddle & Christie-Blick, 1985; Crowell, 1974). Different groups of flower structure on William's Ridge and Broken Ridge indicate relative transpressional and transtensional motion between the Australian and Antarctic plates during the Late Cretaceous and Early Paleogene (Whittaker et al., 2013). We interpret that the flower structures formed in response to local transpressional or transtensional tectonism between the formation

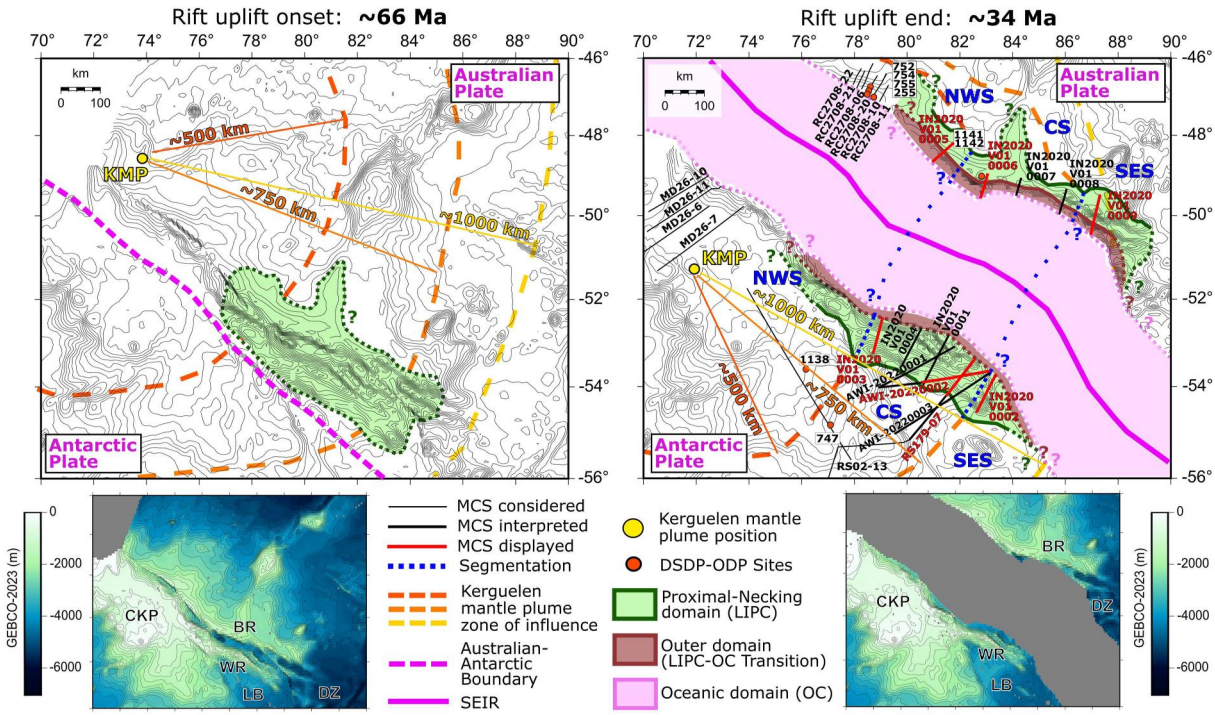

Figure 11. GEBCO, 2023 gridded bathymetric map (GEBCO, 2023) showing the Australian and Antarctic tectonic plates reconstructed at ~66 and ~34 Ma (Whittaker et al., 2013). Contour interval is 250 m. Yellow dot represents the reconstructed position of the Kerguelen mantle plume (O'Neill et al., 2005). Antarctic plate is fixed. Green polygon shows the proximal-necking domain; brown and pink polygons define the outer and oceanic domains, respectively. Dark dashed orange, light dashed orange, and dashed yellow lines mark the approximate extents of different Kerguelen mantle plume influence. Thick dotted purple line and thick solid purple line represent the paleo-position of the Australian-Antarctic boundary and the Southeast Indian Ridge (SEIR), respectively (Whittaker et al., 2013). Thin black lines, thick black lines, and red lines represent MCS profiles considered, analyzed, and shown, respectively, in this study. Blue dotted lines show the boundaries between different segments of the conjugate rifted margins. Orange dots show DSDP-ODP sites. BR, Broken Ridge; CKP, Central Kerguelen Plateau; CS, Central segment; DZ, Diamantina Zone; KMP, Kerguelen mantle plume; LB, Labuan Basin; NWS, Northwest segment; SES, Southeast segment; WR, William's Ridge.

(~100 Ma) and breakup (~44 Ma or after) of WR and BR (Figures 3, 4, and 5–8; Figures S4–S7 in Supporting Information S1).

7. Discussion

7.1. William's Ridge and Broken Ridge Structural Entity: The Proximal-Necking Domain

Rifted margins are usually described through a classification in dichotomies (Peron-Pinvidic & Manatschal, 2019). Building on the traditional "magma-rich"-"magma-poor" rifted margin types, more recent observations defined the concept of deformation migration, originally developed for rifted margins characterized by isostatically balanced continental crust, largely flat and devoid of faults, evolving under a constant extension direction (Peron-Pinvidic et al., 2013). Continental rifted margins are thought to respond to extensional stresses episodically migrating oceanward. Each episode is distinguished by a distinct deformation style, which determines the shape of the lithospheric tectonic features controlled by it. Similar extensional bodies can be grouped and referred to as structural domains (Naliboff et al., 2017; Neuharth et al., 2022; Peron-Pinvidic & Manatschal, 2019; Peron-Pinvidic et al., 2013). To align with this framework, we take into account the complex architecture of the Kerguelen LIP crust. Considering that William's Ridge and Broken Ridge were characterized at Early Paleogene rift onset by an existing high-relief morphology and fault systems inherited from a largely orthogonal Cretaceous rift system, we propose that their LIP crust is characteristic of the proximal and necking domains (Figures 2 and 3–9; Figures S2–S7 in Supporting Information S1). We additionally propose a unique structural domains sequence, as the proximal-necking domain directly abuts the outer domain, with the distal domain absent (Figure 11).

William's Ridge and Broken Ridge are characterized by graben and half-graben geometries in their SES sectors, typical of the proximal domain. However, in their NWS and CS sectors rift shoulders characteristic of the necking domain are predominant (Figures 2, 8, and 9). Similar to structures along Atlantic rifted margins, in the MCS data analyzed in this study we observe extensional deformation structures such as tilted blocks, likely representing the shallower expression of a wedge-shaped crustal domain, and horsts dissected by normal faults, creating accommodation space for the deposition of wedge-shaped sediment layers (Chenin et al., 2022; Peron-Pinvidic et al., 2013) (Figures 3–9; Figures S2–S7 in Supporting Information S1). We therefore associate the formation of William's Ridge and Broken Ridge with processes characteristic of the "stretching" and "thinning" phases of rift development (Chenin et al., 2022; Lavier & Manatschal, 2006; Naliboff et al., 2017; Peron-Pinvidic et al., 2013), or "Phase 1—Distributed deformation" and "Phase 2—Fault system growth" (Neuharth et al., 2022), respectively. The former phase reflects a classical pure shear deformation (McKenzie, 1978), accommodating limited crustal thinning, whereas the latter indicates extreme crustal thinning (Peron-Pinvidic et al., 2013) resulting from detachment faulting (Lister et al., 1986, 1991; Wernicke, 1981; Wernicke & Burchfiel, 1982).

Following formation of the proximal and necking domains, the time progression of archetypal rift systems evolution requires hyperextension/exhumation and magmatism to occur before oceanization (Peron-Pinvidic et al., 2013). However, numerical models show that rift systems with a strong lithosphere as an initial condition tend to be narrow and symmetric, without developing a wide area of hyperextended crust and mantle exhumation (Pérez-Gussinyé et al., 2020). We assume that the hyperextended crust in William's Ridge and Broken Ridge is absent due to these features being predominantly strong, LIP crust. Although the presence of low-angle normal faults (Bell et al., 2018; Lister et al., 1986, 1991; Webber et al., 2018; Wernicke, 1981; Wernicke & Burchfiel, 1982) typically suggests a zone of hyperextended crust (Chenin et al., 2022; Peron-Pinvidic et al., 2013), we propose the low-angle normal faults interpreted in the MCS data set analyzed here to be part of the proximal-necking domain, suggesting formation due to atypical thinning ratios of the lithosphere. The spatial extension of the proximal and necking domains in the archetypal Atlantic rifted margins has been modeled to be ∼200 km in total (Peron-Pinvidic et al., 2013), whereas we propose the LIP crust extension in William's Ridge and Broken Ridge to range between ∼80 and ∼120 km based on satellite-derived and multibeam bathymetric data (GEBCO, 2023), and MCS data (Figures 1, 2, and 3–9; Figures S2–S7 in Supporting Information S1). We propose that the characteristics of the proximal-necking domain are similar on William's Ridge and Broken Ridge because of the apparent symmetry in morphology, which reflects asymmetric evolution processes, of the conjugate margins imaged in the newly presented MCS profiles (Figures 3–9; Figures S2–S8 in Supporting Information S1). Previous studies support asymmetric rifting for Kerguelen Plateau-Broken Ridge conjugate pairs (Karner & Driscoll, 1993; Weissel & Karner, 1989). We explain the apparent symmetry observed here with breakaway zones that can be the result of detachment faults alternating polarity such as observed in the East Africa rift system (Bosworth, 1987; Versfelt & Rosendahl, 1989), the central sector of the Australian-Antarctic margins (Gillard et al., 2015), and the axial valley north of the Fifteen Twenty fracture zone on the Mid-Atlantic Ridge (Cannat et al., 1997) (Figure S8 in Supporting Information S1).

The oceanward boundary of the proximal-necking domain can be recognized where deformation of crust and mantle lithosphere changes from being decoupled to coupled (Peron-Pinvidic et al., 2013). On the MCS data interpreted here, the penetration depth below the seafloor is limited to ∼2 s TWT (Figures 3–9; Figures S2–S7 in Supporting Information S1), therefore limiting observation of deep structures showing interactions between the crust and mantle lithosphere. However, magnetic anomaly identifications allow us to speculate on the progression of rifted margin domains. Magnetic anomaly identifications are evidence of oceanic crustal emplacement at the mid-ocean ridge and seafloor spreading (Vine & Matthews, 1963; Williams et al., 2013) Nonetheless, magnetic anomalies have been picked in transitional areas between continental and oceanic crust, for example, in the CS of the Australian-Antarctic rifted margins (Gillard et al., 2015; Whittaker et al., 2007). We use here magnetic anomaly picks (Ségoufin et al., 2004) for defining the boundary between LIP crust emplaced by the Kerguelen mantle plume and characterizing the proximal-necking domain, and the zone of transition to normal oceanic crust, emplaced through seafloor spreading at the SEIR and defining the outer and oceanic domains (Figures 1, 2, and 10). On Broken Ridge we observe a transitional zone between LIP crust and oceanic crust which is typical of the outer domain (LIPC-OC Transition in Figures 4, 6, and 9; Figures S4 and S6 in Supporting Information S1) (Peron-Pinvidic et al., 2013). We therefore identify the outer domain on Broken Ridge, although we do not propose a magmatic phase (Peron-Pinvidic et al., 2013) due to no identifiable syn-rift magmatism on the MCS

data (Figures 3–9; Figures S2–S7 in Supporting Information S1). Although not observed on MCS data on William's Ridge, we also propose an outer domain on this conjugate margin, building on the idea of an apparent symmetric rift system (Karner & Driscoll, 1993; Pérez-Gussinyé et al., 2020) (Figure S8 in Supporting Information S1).

7.2. Magma-Poor Rifted Margins in a Mantle Plume Context

William's Ridge and Broken Ridge show little seismic evidence of magmatism affecting the pre-rift foundations and syn-rift sedimentary packages (Figures 3–9; Figures S2–S7 in Supporting Information S1). This observation is somewhat unexpected given the <1,000 km proximity to the active Kerguelen plume during rifting and breakup and contradicts the concept of magma-rich rifted margins forming if a mantle plume is proximal during lithospheric rifting and breakup (Geoffroy, 2005; Tomasi et al., 2021). The only evidence for effusive magmatism affecting William's Ridge is the dipping reflections imaged within igneous basement (Figures 3 and 7; Figures S2 and S3 in Supporting Information S1) (Borissova et al., 2002). These are similar to reflections observed on the Agulhas Plateau (Parsiegla et al., 2008; Uenzelmann-Neben et al., 1999), Kerguelen Plateau (Coffin et al., 1990; Schaming & Rotstein, 1990), Manihiki Plateau (Pietsch & Uenzelmann-Neben, 2015), Ontong Java Plateau (Inoue et al., 2008), and Shatsky Rise (Zhang et al., 2015); their interpretation as lava flows is consistent for all these oceanic plateaus.

Although analogies can be made between dipping reflections observed in this study and SDRs imaged in magma-rich rift systems (Backman et al., 1984; Callot et al., 2002; Geoffroy, 2005; Gohl et al., 2011; Peron-Pinvidic & Osmundsen, 2018; Tomasi et al., 2021), they differ in key characteristics. Establishing the area and volume encompassed by dipping reflections is hindered by the lack of penetration in the MCS data analyzed in this study, with the exception of Line RS179-07 (Figure 3), and therefore on making a thorough comparison with other SDRs. However, intra-basement reflections imaged on William's Ridge apparently dip southwest, which is the opposite direction with respect to the SEIR and paleo-spreading center. In addition, other intra-basement reflections, previously identified elsewhere on the Kerguelen Plateau, not only vary significantly in apparent dips, but also have syncline and anticline shapes (Coffin et al., 1990; Colwell et al., 1988; Planke et al., 2000; Schaming & Rotstein, 1990), marking a significant contrast with SDRs on magma-rich rifted margins. Therefore, due to their apparent dip away from the rifting and breakup locus, and their presence exclusively within igneous basement (Figures 3 and 7; Figures S2 and S3 in Supporting Information S1), we propose that the intra-basement dipping reflections imaged on William's Ridge are not syn-rift SDRs, and were formed during LIP emplacement (pre-rift) presumably as subaerial landward flows (Planke et al., 2000). Alternatively, the intra-basement dipping reflections may represent SDRs emplaced during the opening of the Labuan Basin. On the conjugate central CKP margin, a paucity of deep penetration MCS data precludes confirming or denying the existence of similar intrabasement dipping reflections (Borissova et al., 2002). Considering that SDRs constitute primary evidence for classifying a rift system as "magma-rich," we interpret the William's Ridge-Broken Ridge conjugate rifted margins to be "magma-poor" (Biari et al., 2021; T. Doré & Lundin, 2015; Franke, 2013; Lavier & Manatschal, 2006; Manatschal, 2004; Peron-Pinvidic & Manatschal, 2019; Sutra & Manatschal, 2012).

Why rifting and breakup of William's Ridge and Broken Ridge did not involve significant magmatism is likely because most magma upwelling from the plume conduit had been exploiting lithospheric fractures in the Indian plate and forming the Ninetyeast Ridge from ~82 Ma (Coffin et al., 2002; Khogenkumar et al., 2022; Mahoney et al., 1983; Weissel et al., 1991). We suggest that most magma was conveyed away from the William's Ridge-Broken Ridge region, thus inhibiting magmatism coeval with rifting and breakup. Although weaker and magmatically less productive than the Kerguelen mantle plume, the Marquesas hotspot has been similarly modeled to exploit pre-existing lithospheric weaknesses, although not being sufficiently strong to penetrate normal oceanic lithosphere (McNutt et al., 1989).

7.3. Factors Controlling Lateral Segmentation of William's Ridge and Broken Ridge

Along-strike segmentation in continental rift settings has been explained by transfer faults which define the mechanism of offset between systems governed by discrete fault systems (Gibbs, 1984). This concept has been further applied to continental rifted margins (Acocella et al., 2005; Lister et al., 1986). Although generalization of the concept plays an important role in understanding how rift systems evolve in three dimensions, the trigger and

cause of lateral segmentation remains incompletely known (A. Doré et al., 1999; Peron-Pinvidic & Osmundsen, 2018).

Margin segmentation observed in the North Atlantic rift system (Osmundsen & Péron-Pinvidic, 2018; Peron-Pinvidic & Osmundsen, 2018) has been explained through the response of breakaway complexes to extensional stresses (Axen, 2004). Breakaway complexes are lateral boundaries of structural domains, connected through combined major fault groups. The change of role of these controlling faults (e.g., fault jumps) activates distinct deformation phases (Naliboff et al., 2017; Neuharth et al., 2022) along discrete sectors along strike of the margins, leading to the creation of offsets. In this study, we do not observe offsets between proximal-necking, outer, and oceanic domains, yet we recognize groups of major tectonic features, belonging to the proximal-necking domain, changing characteristics along the strikes of William's Ridge and Broken Ridge (Figures 3–9; Figures S2–S7 in Supporting Information S1). We therefore describe the lateral segmentation focusing on the observed main structural blocks instead of each controlling fault constituting part of the system (Osmundsen & Péron-Pinvidic, 2018; Peron-Pinvidic & Osmundsen, 2018). A predominant rift shoulder consistently represents the NWS and CS. However, the adjacent platform structure in the former (Figure 5), and a tilted and rotated block in the latter (Figures 3, 5–7; Figures S2–S7 in Supporting Information S1), are distinctive tectonic features requiring a different classification for the two segments. The SES is dominated by horsts and half-grabens (Figures 8 and 9).

We propose that the Kerguelen mantle plume swell and inherited post-emplacement lithospheric structures of the Cretaceous Kerguelen Plateau-Broken Ridge LIP control the lateral segmentation of William's Ridge and Broken Ridge (Figure 11). The plume underlay the India-Australia-Antarctica triple junction between ∼66 and ∼59 Ma, and the CKP between ∼58 and ∼34 Ma (O'Neill et al., 2005; Whittaker et al., 2013), likely influencing the vertical movements of William's Ridge and Broken Ridge without manifesting any volcanism in the area, due to the obstructing strong and thick LIP crust characterizing the conjugate margins (Gladczenko & Coffin, 2001; MacKenzie et al., 1980). The NWS and CS fall within a ∼500 and ∼500–750 km radius, respectively, from the proposed Kerguelen plume center. In contrast, the SES is ∼750–1,000 km from the proposed Kerguelen plume center (Figure 11). Conceptual models of mantle plume shape show the mantle plume head deepening from its central axis toward its edges (e.g., Griffiths & Campbell, 1991; Koppers et al., 2021). Although the mantle plume head temperature remains generally constant over its surface, the offset between the central axis position and the edges position may influence the amount of heat diffused toward different parts of the impinged lithosphere. Evidence supporting rifted margin LIP crust thinning with distance from the center of the emplacement (Coffin & Eldholm, 1994) is deepening blocks and horsts toward the southeast on William's Ridge, and toward the east on Broken Ridge (Figures 3–9; Figures S2–S7 in Supporting Information S1) imaged by our MCS and multibeam bathymetry data.

7.3.1. The NWS—Strong Kerguelen Mantle Plume Influence and Strong Deformation

On the NWS (Figure 11), the hotspot is characterized by strong impingement forces and high heat diffusion toward the lithosphere (Hartley et al., 2011; Hill et al., 1992; Koppers et al., 2021; Whittaker et al., 2015) acting on relatively thin LIP crust (Coffin & Eldholm, 1994). The result is formation of a rift shoulder and a wedge-shaped layered sediment package at least ∼25 km wide (Figure 4). In this segment, the LIP crust transitions to oceanic crust thicknesses (Coffin & Eldholm, 1994; Crameri et al., 2019) in response to rift-induced stresses through a relatively high degree of rotation. The result is the generation of low-angle normal faults with a true dip of ∼25° imaged on the multibeam bathymetry and MCS data (Figures 2 and 4).

7.3.2. The CS—Evolution Through Distinct Types of Flexural Rotation

On the CS (Figure 11), the impingement forces and heat diffusion of the Kerguelen hotspot toward the lithosphere likely decreased to moderate (Hartley et al., 2011; Hill et al., 1992; Koppers et al., 2021; Whittaker et al., 2015). The Kerguelen mantle plume here impinged on LIP crust a few km thinner than the one on the NWS (Coffin & Eldholm, 1994). Although influence of the Kerguelen mantle plume is weaker in this segment, the relatively thinner crust of William's Ridge and Broken Ridge played an important role in the formation of tectonic features similar to the NWS, such as a predominant rift shoulder and chaotic to layered seismic patterns on both conjugate margins (Figures 3–9; Figures S2–S7 in Supporting Information S1). On Broken Ridge, we speculate that the difference between the platform-shaped area on the NWS (Figure 5), and the tilted and rotated blocks on the CS (Figure 6; Figures S4 and S6 in Supporting Information S1), is related to inherited characteristics of the crust, such

as regional zones of weakness and fault systems. The displacement of the LIP crust of William's Ridge, characterized by lower degree of flexural rotation than Broken Ridge (Buck, 1988; Karner & Driscoll, 1993), resulted in the creation of blocks predominantly characterized by normal faults with true dips between 26° and 30° (Figures 2, 3, 5, and 7; Figures S2, S3, S5, and S7 in Supporting Information S1). Experiencing similar regional deformation, the LIP crust of Broken Ridge generated similar low-angle normal faults, although with true dips ranging between 25° and 27° (Figures 2 and 6; Figures S4 and S6 in Supporting Information S1).

7.3.3. The SES—Boundary of LIP Crust and Kerguelen Mantle Plume Influence

The boundary between the CS and SES (Figures 2 and 11) marks an abrupt change in the structural characteristics of William's Ridge and Broken Ridge. On the SES, the impingement forces and heat diffusion of the Kerguelen hotspot toward the lithosphere are proposed to be low, as the SES is proximal to the edge of the hotspot's radius of influence (Hartley et al., 2011; Hill et al., 1992; Koppers et al., 2021; Whittaker et al., 2015). Simultaneously, the SES LIP crust subject to mantle plume impingement is a few km thinner compared to the CS, as its southeastern boundary marks the edge of the Kerguelen LIP (Coffin & Eldholm, 1994). The combination of mantle plume impingement and pre-existing lithospheric conditions led to the creation of horsts and half-grabens and well-stratified uppermost seismic units (Figures 8 and 9). Consistent with stress accommodation responses on the CS, the SES developed steeper low-angle normal faults on William's Ridge (~27°, Figures 2 and 8) compared to Broken Ridge (~25°, Figures 2 and 9).

7.4. Transform Motion Component in the Australian-Antarctic Rift System

Previous publications propose little to no relative motion between Broken Ridge and the CKP during Late Cretaceous-Early Cenozoic time, with any motion accommodated by stretching and extension (Borissova et al., 2002; Rotstein et al., 1992), and only a negligible component of left-lateral strike-slip motion (Munschy et al., 1993). In contrast, Whittaker et al. (2013) proposed a broadly strike-slip boundary, oriented northwest-southeast, through the Kerguelen region to accommodate broader Australian-Antarctic plate motions (Figure S1 in Supporting Information S1). Transtensional motion along the CKP-Broken Ridge boundary between ~100 and ~44 Ma has been modeled to have resulted in a ~50 km separation of the two (Whittaker et al., 2013). During this time interval, the Kerguelen mantle plume likely had positive feedback on the William's Ridge and Broken Ridge lithospheric weakening, transferring heat within the space progressively created between the conjugate margins by transtensional motion. This mechanism likely enabled the boundary jump at ~44 Ma (Whittaker et al., 2013) (Figure S1 in Supporting Information S1). We therefore speculate that the Kerguelen mantle plume played a significant role in maximizing transtensional motion and therefore jointly controlling the formation of tectonic structures observed on the rifted margins. Our MCS interpretations, combined with satellite-derived (GEBCO, 2023) and multibeam bathymetry data (Beaman, 2023; Coffin et al., 2023a; Picard et al., 2018), enable us to propose almost purely strike-slip motion between the Kerguelen Plateau and Broken Ridge in Late Cretaceous-Early Cenozoic time (Whittaker et al., 2013).

To test the proposed idea of predominantly transform motion between Broken Ridge, on the Australian plate, and Williams Ridge, on the Antarctic plate, we examine the 3D extension of fault systems, along with the characteristics of flower structures on bathymetric and MCS data. Numerous relay ramps, pull-apart basins, and flower structures (Figures 3–10; Figures S2–S7 in Supporting Information S1) are consistent with the Kerguelen sector of the Australian-Antarctic boundary being broadly transform from Late Cretaceous time to at least ~44 Ma. The dominant transform stresses acting on the once-contiguous end members explain the creation of relay ramps, similarly to what observed in East Quantoxhead, UK, Rio de Peixe Basin, northeast Brazil, Newport-Inglewood Trend, California, and in the Bovey Basin SW England (Peacock & Sanderson, 1995). In addition, pull-apart basins can be attributed to strike-slip motion, comparable to models of Death Valley, California (Burchfiel & Stewart, 1966; Mann et al., 1983). Limitations in density and resolution of the MCS data prevent a thorough correlation of flower structures along the strike of the conjugate William's Ridge-Broken Ridge margins. However, the relay ramps, pull-apart basins, and flower structures in the MCS and bathymetric data confirm the broad transform motion of the Kerguelen sector during Late Cretaceous-Early Cenozoic time (Whittaker et al., 2013). Positive and negative flower structures suggest the presence of localized depocenters indicating syn-rift transpressional and transtensional motion between William's Ridge and Broken Ridge (Figures 3, 4, and 5–8; Figures S4–S7 in Supporting Information S1).

8. Conclusions

In this study, we attempt to understand how the William's Ridge-Broken Ridge rift aligns with the deformation migration classification for rifted margins. In addition, we investigate how the observed along-strike segmentation on the conjugate end members reflects the influence that the Kerguelen mantle plume might have had on the LIP lithosphere during rifting. Moreover, we test the syn-rift transform motion modeled for the Australian and Antarctic plates during Late Cretaceous-Early Paleogene time using the observed tectonic structures identified in the dataset presented.

Interpretation of MCS profiles reveals the presence of grabens and half-graben structures, tilted blocks representing the shallower expression of a wedge-shaped crustal domain, low-angle normal faults, and wedge-shaped sedimentary packages, characteristic of combined proximal and necking domain zonation on William's Ridge and Broken Ridge. Magnetic anomalies help define the boundary between LIP crust emplaced by the Kerguelen mantle plume, and oceanic crust emplaced at the SEIR through normal seafloor spreading. Different sectors of oceanic crust characterized by different thicknesses correspond to abrupt transitions between structural entities. The LIP crust forms the proximal-necking domain, whereas the thinner oceanic crust forms the outer and oceanic domains.

In stark contrast to the usual "magma-rich" rifted margins located in the vicinity of a mantle plume, we propose a "magma-poor" model for the William's Ridge and Broken Ridge rift system. Based on analysis of MCS profiles on the conjugate margins, we relate the absence of magmatism, that is, no SDRs, to Kerguelen mantle plume output being focussed at the Ninetyeast Ridge.

The combination of the MCS data, information about relative thicknesses and flexural response of LIP crust of William's Ridge and Broken Ridge, reconstructions of tectonic plates, and the location of the Kerguelen mantle plume enables us to consider how segmentation of the conjugate rifted margins evolved. We propose a model consisting of three sectors of mantle plume influence on William's Ridge and Broken Ridge, which correspond to zones of distinct inherited LIP crustal thicknesses. The northwest segment (NWS), central segment (CS) and the southeast segment (SES), are, respectively, highly, moderately, and slightly affected by the Kerguelen hotspot.

Relay-ramps, pull-apart basins and flower structures on bathymetric data and MCS profiles support the hypothesis of consistent relative sinistral transform motion, between the Australian and Antarctic plates, between Late Cretaceous and Early Paleogene time (~100 to ~44 Ma). The transtensional motion was likely magnified through heat diffusion below the weakened LIP lithosphere by the Kerguelen mantle plume.

Data Availability Statement

The bathymetric and multichannel seismic reflection data presented in this study are available for download via the Australian Antarctic Division (AAD) portal (https://data.aad.gov.au/metadata/AAS_4519_IN2020_V01_MCS) (Coffin et al., 2023c), Geoscience Australia website (https://ecat.ga.gov.au/geonetwork/srv/eng/catalog.search#/metadata/147703) (Beaman, 2023), Research Data Australia website (https://doi.org/10.25919/5f7e3bcfe68e8; https://doi.org/10.25919/5f7e3b93126ea) (Coffin et al., 2023a, 2023b) and PANGAEA portal (https://doi.pangaea.de/10.1594/PANGAEA.916165; https://doi.pangaea.de/10.1594/PANGAEA.922556; https://doi.pangaea.de/10.1594/PANGAEA.934739; https://doi.pangaea.de/10.1594/PANGAEA.935731) (Dreutter et al., 2020; Uenzelmann-Neben, 2020, 2021a, 2021b).

The multichannel seismic reflection data have been processed and interpreted using PETROSYS (GLOBE Claritas—version V7-1-1: https://www.petrosys.com.au), IHS Markit (IHS Kingdom—version 2020: https://kindgom.ihs.com), Paradigm software (Release 19)—Emerson E&P software, Emerson Automation Solutions (https://www.emerson.com/en-us/news/automation/2001-exploration-production-software-paradigm). Each software is available via license.

Acknowledgments

The authors thank the captains and crews of RV *Investigator* and RV *Sonne,* and the support personnel of CSIRO-MNF and AWI for the organization and assistance of the voyages IN2020_V01 and SO272, respectively. We acknowledge the grant of sea time on RV *Investigator* in undertaking this research and the use of the CSIRO Marine National Facility (https://ror.org/01mae9353). We appreciate the support of Australian Antarctic Science Program Grant 4915. We thank PETROSYS (GLOBE Claritas) for providing the seismic data processing software, and IHS Markit, for providing the seismic data interpretation software IHS Kingdom. The authors thank Emerson E&P software, Emerson Automation Solutions, for providing licenses for their seismic processing and mapping software Paradigm in the scope of the Emerson Academic program. The figures in this paper were made with the open-source software Generic Mapping Tool (Version 6.1.1) (Wessel et al., 2019) and Inkscape (Version 1.1—https://inkscape.org/). We thank Ian James and Michal Wenderlich for the support with seismic data processing, Matthias Schneider for the processing of RV *Sonne* SO272 (2020) seismic data, and Isabel Sauermilch for helpful discussions. We greatly appreciate the insightful and constructive comments of Editor I. Manighetti, the Associate Editor, and two anonymous reviewers. LM's PhD scholarship is supported by Geoscience Australia. LM and KH acknowledge support by the Australian Research Council Special Research Initiative, Australian Centre for Excellence in Antarctic Science (Project Number SR200100008). SW acknowledges funding support by the ARC Grant DP200100966. MFC is grateful for the support of the Detached Cultural Organization. The SO272 research voyage and the Kerguelen Plateau Sediment Drift project were funded by the German Federal Ministry of Education and Research (BMBF) under project 03G0272A. Additional funding has been provided by the Alfred-Wegener-Institut Helmholtz-Zentrum für Polar- und Meeresforschung. Open access publishing facilitated by University of Tasmania, as part of the Wiley - University of Tasmania agreement via the Council of Australian University Librarians.

References

Acocella, V., Morvillo, P., & Funiciello, R. (2005). What controls relay ramps and transfer faults within rift zones? Insights from analogue models. *Journal of Structural Geology*, *27*(3), 397–408. https://doi.org/10.1016/j.jsg.2004.11.006

Argus, D. F., Gordon, R. G., & DeMets, C. (2011). Geologically current motion of 56 plates relative to the no-net-rotation reference frame. *Geochemistry, Geophysics, Geosystems*, *12*(11), Q11001. https://doi.org/10.1029/2011GC003751

Axen, G. J. (2004). Mechanics of low-angle normal faults. In *Rheology and deformation of the lithosphere at continental margins* (pp. 46–91). https://doi.org/10.7312/karn12738-004

Backman, J., Morton, A., & Murray, L. J. (1984). Evolution of volcanic rifted margins: Synthesis of Leg 81 results on the west marginof Rockall Plateau. In *Proceedings of the DSDP, Initial Reports, 81: College Station, TX (Ocean Drilling Program)* (pp. 883–911). https://doi.org/10.2973/dsdp.proc.81.139.1984

Barron, J. A., Baldauf, J. G., Barrera, E., Caulet, J.-P., Huber, B. T., Keating, B. H., et al. (1991). Biochronologic and magnetochronologic synthesis of Leg 119 sediments from the Kerguelen Plateau and Prydz Bay, Antarctica. In *Proceedings of the ODP, Initial Reports, 119: College Station, TX (Ocean Drilling Program)* (pp. 813–847). https://doi.org/10.2973/odp.proc.sr.119.188.1991

Barron, J. A., Larsen, B., & Baldauf, J. G. (1989). Leg 119 preliminary report. In *Proceedings of the ODP, Initial Reports, 119: College Station, TX (Ocean Drilling Program)* (pp. 1–67). https://doi.org/10.2973/odp.proc.ir.119.1989

Beaman, R. J. (2023). Kerguelen Plateau 100 m bathymetry grid compilation (20220004C) [Dataset]. Geoscience Australia, Canberra. https://doi.org/10.26186/147703

Bell, R. E., Duclaux, G., Nixon, C. W., Gawthorpe, R. L., & McNeill, L. C. (2018). High-angle, not low-angle, normal faults dominate early rift extension in the Corinth Rift, Central Greece. *Geology*, *46*(2), 115–118. https://doi.org/10.1130/G39560.1

Bénard, F., Callot, J.-P., Vially, R., Schmitz, J., Roest, W., Patriat, M., & Loubrieu, B. (2010). The Kerguelen plateau: Records from a long-living/composite microcontinent. *Marine and Petroleum Geology*, *27*(3), 633–649. https://doi.org/10.1016/j.marpetgeo.2009.08.011

Berggren, W. A., Kent, D. V., & Flynn, J. J. (1985). Jurassic to Paleogene: Part 2 Paleogene geochronology and chronostratigraphy. *Geological Society, London, Memoirs*, *10*(1), 141–195. https://doi.org/10.1144/GSL.MEM.1985.010.01.15

Berggren, W. A., Kent, D. V., Flynn, J. J., & Van Couvering, J. A. (1985). Cenozoic geochronology. *Geological Society of America Bulletin*, *96*(11), 1407–1418. https://doi.org/10.1130/0016-7606(1985)96<1407:CG>2.0.CO;2

Berggren, W. A., Kent, D. V., & Van Couvering, J. A. (1985). The Neogene: Part 2 Neogene geochronology and chronostratigraphy. *Geological Society, London, Memoirs*, *10*(1), 211–260. https://doi.org/10.1144/GSL.MEM.1985.010.01.18

Beslier, M.-O., Royer, J.-Y., Girardeau, J., Hill, P. J., Boeuf, E., Buchanan, C., et al. (2004). Une large transition continent-ocean en pied de marge sud-ouest australienne: Premiers resultats de la campagne MARGAU/MD110. *Bulletin de la Société Géologique de France*, *175*(6), 629–641. https://doi.org/10.2113/175.6.629

Biari, Y., Klingelhoefer, F., Franke, D., Funck, T., Loncke, L., Sibuet, J.-C., et al. (2021). Structure and evolution of the Atlantic passive margins: A review of existing rifting models from wide-angle seismic data and kinematic reconstruction. *Marine and Petroleum Geology*, *126*, 104898. https://doi.org/10.1016/j.marpetgeo.2021.104898

Biddle, K. T., & Christie-Blick, N. (1985). Glossary—Strike-slip deformation, basin formation and sedimentation. In K. T. Biddle & N. Christie-Blick (Eds.), *Strike-slip deformation, basin formation and sedimentation* (Vol. 37, pp. 375–386). SEPM Special Publication.

Borissova, I., Coffin, M. F., Charvis, P., & Operto, S. (2003). Structure and development of a microcontinent: Elan bank in the southern Indian ocean. *Geochemistry, Geophysics, Geosystems*, *4*(9), 1071. https://doi.org/10.1029/2003GC000535

Borissova, I., Moore, A., Sayers, J., Parums, R., Coffin, M., & Symonds, P. (2002). Geological framework of the Kerguelen Plateau and adjacent ocean basins. In *Geoscience Australia, Canberra, record 2002/05* (pp. 1–78).

Bosworth, W. (1987). Off-axis volcanism in the Gregory rift, east Africa: Implications for models of continental rifting. *Geology*, *15*(5), 397–400. https://doi.org/10.1130/0091-7613(1987)15<397:ovitgr>2.0.co;2

Boyden, J. A., Müller, R. D., Gurnis, M., Torsvik, T. H., Clark, J. A., Turner, M., et al. (2011). *Next-generation plate-tectonic reconstructions using GPlates* (pp. 95–113). Cambridge University Press. https://doi.org/10.1016/j.earscirev.2020.103477

Buck, W. R. (1988). Flexural rotation of normal faults. *Tectonics*, *7*(5), 959–973. https://doi.org/10.1029/tc007i005p00959

Buck, W. R. (2007). Dynamic processes in extensional and compressional settings: The dynamics of continental breakup and extension. *Crust and Lithosphere Dynamics*, *6*, 335–376. https://doi.org/10.1016/B978-044452748-6.00110-3

Burchfiel, B. C., & Stewart, J. (1966). "Pull-apart" origin of the central segment of Death Valley, California. *Geological Society of America Bulletin*, *77*(4), 439–442. https://doi.org/10.1130/0016-7606(1966)77[439:pootcs]2.0.co;2

Callot, J. P., Geoffroy, L., & Brun, J. P. (2002). Development of volcanic passive margins: Three-dimensional laboratory models. *Tectonics*, *21*(6), 2-1–2-13. https://doi.org/10.1029/2001tc901019

Campbell, I. H., & Griffiths, R. W. (1990). Implications of mantle plume structure for the evolution of flood basalts. *Earth and Planetary Science Letters*, *99*(1–2), 79–93. https://doi.org/10.1016/0012-821x(90)90072-6

Cande, S. C., & Mutter, J. C. (1982). A revised identification of the oldest sea-floor spreading anomalies between Australia and Antarctica. *Earth and Planetary Science Letters*, *58*(2), 151–160. https://doi.org/10.1016/0012-821x(82)90190-x

Cannat, M., Lagabrielle, Y., Bougault, H., Casey, J., de Coutures, N., Dmitriev, L., & Fouquet, Y. (1997). Ultramafic and gabbroic exposures at the Mid-Atlantic Ridge: Geological mapping in the 15°N region. *Tectonophysics*, *279*(1–4), 193–213. https://doi.org/10.1016/s0040-1951(97)00113-3

Chao, P., Manatschal, G., Chenin, P., Ren, J., Zhang, C., Pang, X., et al. (2021). The tectono-stratigraphic and magmatic evolution of conjugate rifted margins: Insights from the NW South China Sea. *Journal of Geodynamics*, *148*, 101877. https://doi.org/10.1016/j.jog.2021.101877

Charvis, P., Recq, M., Operto, S., & Brefort, D. (1995). Deep structure of the northern Kerguelen Plateau and hotspot-related activity. *Geophysical Journal International*, *122*(3), 899–924. https://doi.org/10.1111/j.1365-246X.1995.tb06845.x

Chenin, P., Manatschal, G., Ghienne, J. F., & Chao, P. (2022). The syn-rift tectono-stratigraphic record of rifted margins (Part II): A new model to break through the proximal/distal interpretation Frontier. *Basin Research*, *34*(2), 489–532. https://doi.org/10.1111/bre.12628

Close, D. I., Watts, A., & Stagg, H. (2009). A marine geophysical study of the Wilkes Land rifted continental margin, Antarctica. *Geophysical Journal International*, *177*(2), 430–450. https://doi.org/10.1111/j.1365-246X.2008.04066.x

Coffin, M., Edwards, S., Kuna, N., & Navidad, C. (2023a). IN2020_V01 Broken Ridge bathymetry 200m resolution AusSeabed products [Dataset]. Research Data Australia. https://doi.org/10.25919/5f7e3b93126ea

Coffin, M., Edwards, S., Kuna, N., & Navidad, C. (2023b). IN2020_V01 Williams Ridge bathymetry 100 m resolution AusSeabed products [Dataset]. CSIRO Data Access Portal. https://doi.org/10.25919/5f7e3bcfe68e8

Coffin, M., Frey, F., & Wallace, P. (2000). Development of an intraoceanic large igneous province: The Kerguelen Plateau and Broken Ridge, southern Indian Ocean. In *Proceedings of the ODP, Initial Reports, 183: College Station, TX (Ocean Drilling Program), No. 1* (Vol. 26, pp. 5–9). https://doi.org/10.2973/odp.proc.ir.183.2000

Coffin, M., Magri, L., & Whittaker, J. (2023c). IN2020_V01—Multichannel seismic reflection (MCS) dataset, version 1 [Dataset]. Australian Antarctic Data Centre. https://doi.org/10.26179/qe01-db93

Coffin, M. F. (1992). Subsidence of the Kerguelen Plateau: The Atlantis concept. In *Proceedings of the ODP, Science Results, 120: College Station, TX (Ocean Drilling Program)* (pp. 945–949). https://doi.org/10.2973/odp.proc.sr.120.202.1992

Coffin, M. F., Davies, H. L., & Haxby, W. F. (1986). Structure of the Kerguelen Plateau province from SEASAT altimetry and seismic reflection data. *Nature*, *324*(6093), 134–136. https://doi.org/10.1038/324134a0

Coffin, M. F., & Eldholm, O. (1994). Large igneous provinces: Crustal structure, dimensions, and external consequences. *Reviews of Geophysics*, *32*(1), 1–36. https://doi.org/10.1029/93rg02508

Coffin, M. F., Munschy, M., Colwell, J. B., Schlich, R., Davies, H. L., & Li, Z.-G. (1990). Seismic stratigraphy of the Raggatt Basin, southern Kerguelen Plateau: Tectonic and paleoceanographic implications. *Geological Society of America Bulletin*, *102*(5), 563–579. https://doi.org/10.1130/0016-7606(1990)102<0563:ssotrb>2.3.co;2

Coffin, M. F., Pringle, M. S., Duncan, R. A., Gladczenko, T. P., Storey, M., Muller, R. D., & Gahagan, L. (2002). Kerguelen hotspot magma output since 130 Ma. *Journal of Petrology*, *43*(7), 1121–1137. https://doi.org/10.1093/petrology/43.7.1121

Colwell, J., Coffin, M., Pigram, C., Davies, H., Stagg, H., & Hill, P. (1988). Seismic stratigraphy and evolution of the Raggatt Basin, southern Kerguelen Plateau. *Marine and Petroleum Geology*, *5*(1), 75–81. https://doi.org/10.1016/0264-8172(88)90041-4

Crameri, F., Conrad, C. P., Montési, L., & Lithgow-Bertelloni, C. R. (2019). The dynamic life of an oceanic plate. *Tectonophysics*, *760*, 107–135. https://doi.org/10.1016/j.tecto.2018.03.016

Crowell, J. C. (1974). Origin of late Cenozoic basins in southern California. In *Tectonics and sedimentation, special publication* (Vol. 22, pp. 190–204).

Cunningham, W., & Mann, P. (2007). Tectonics of strike-slip restraining and releasing bends. *Geological Society, London, Special Publications*, *290*(1), 1–12. https://doi.org/10.1144/SP290.1

Davies, T., Luyendyk, B., Kevin, S., Kempre, D., McKelvey, B., Leidy, R., et al. (1974). *Initial reports of the Deep Sea Drilling project* (Vol. 26, p. 1129). U.S. Government Printing Office.

Davy, B., Hoernle, K., & Werner, R. (2008). Hikurangi Plateau: Crustal structure, rifted formation, and Gondwana subduction history. *Geochemistry, Geophysics, Geosystems*, *9*(7), 1–31. https://doi.org/10.1029/2007GC001855

DeMets, C., Gordon, R. G., & Argus, D. F. (2010). Geologically current plate motions. *Geophysical Journal International*, *181*(1), 1–80. https://doi.org/10.1111/j.1365-246X.2009.04491

Dick, H. J., Lin, J., & Schouten, H. (2003). An ultraslow-spreading class of ocean ridge. *Nature*, *426*(6965), 405–412. https://doi.org/10.1038/nature02128

Direen, N. G., Stagg, H. M., Symonds, P. A., & Colwell, J. B. (2011). Dominant symmetry of a conjugate southern Australian and East Antarctic magma-poor rifted margin segment. *Geochemistry, Geophysics, Geosystems*, *12*(2), 1–29. https://doi.org/10.1029/2010GC003306

Doré, A., Lundin, E., Jensen, L., Birkeland, Ø., Eliassen, P., & Fichler, C. (1999). Principal tectonic events in the evolution of the northwest European Atlantic margin. *Geological Society of London*, *5*(1), 41–61. https://doi.org/10.1144/0050041

Doré, T., & Lundin, E. (2015). Research focus: Hyperextended continental margins—Knowns and unknowns. *Geology*, *43*(1), 95–96. https://doi.org/10.1130/focus012015.1

Doubrovine, P. V., Steinberger, B., & Torsvik, T. H. (2012). Absolute plate motions in a reference frame defined by moving hot spots in the Pacific, Atlantic, and Indian oceans. *Journal of Geophysical Research*, *117*(9), 1–30. https://doi.org/10.1029/2011JB009072

Dreutter, S., Hehemann, L., Werner, E., & Uenzelmann-Neben, G. (2020). Multibeam bathymetry raw data (Kongsberg EM 122 entire dataset) of RV SONNE during cruise SO272 [Dataset]. PANGAEA. https://doi.org/10.1594/PANGAEA.916165

Driscoll, N. W., Karner, G. D., & Weissel, J. (1991). Stratigraphic response of carbonate platforms and terrigenous margins to relative sea-level changes: Are they really that different? In *Proceedings of the ODP, Science Results, 121: College Station, TX (Ocean Drilling Program)* (pp. 743–761). https://doi.org/10.2973/odp.proc.sr.121.178.1991

Duncan, R., Falloon, T., Quilty, P., & Coffin, M. (2016). Widespread Neogene volcanism on central Kerguelen Plateau, southern Indian ocean. *Australian Journal of Earth Sciences*, *63*(4), 379–392. https://doi.org/10.1080/08120099.2016.1221857

Duncan, R. A. (2002). A time frame for construction of the Kerguelen Plateau and Broken Ridge. *Journal of Petrology*, *43*(7), 1109–1119. https://doi.org/10.1093/petrology/43.7.1109

Eldholm, O., Thiede, J., & Taylor, E. (1989). The Norwegian continental margin: Tectonic, volcanic, and paleoenvironmental framework. In *Proceedings of the ODP, Science Results, 104: College Station, TX (Ocean Drilling Program)* (pp. 5–26). https://doi.org/10.2973/odp.proc.sr.104.110.1989

Espurt, N., Callot, J. P., Roure, F., Totterdell, J. M., Struckmeyer, H. I., & Vially, R. (2012). Transition from symmetry to asymmetry during continental rifting: An example from the bight basin–Terre Adélie (Australian and Antarctic conjugate margins). *Terra Nova*, *24*(3), 167–180. https://doi.org/10.1111/j.1365-3121.2011.01055.x

Falvey, D. A. (1974). The development of continental margins in plate tectonic theory. *The Australian Petroleum Exploration Association Journal*, *14*(1), 95–106. https://doi.org/10.1071/aj73012

Franke, D. (2013). Rifting, lithosphere breakup and volcanism: Comparison of magma-poor and volcanic rifted margins. *Marine and Petroleum Geology*, *43*, 63–87. https://doi.org/10.1016/j.marpetgeo.2012.11.003

Franke, D., Savva, D., Pubellier, M., Steuer, S., Mouly, B., Auxietre, J.-L., et al. (2014). The final rifting evolution in the South China Sea. *Marine and Petroleum Geology*, *58*(B), 704–720. https://doi.org/10.1016/j.marpetgeo.2013.11.020

Frey, F., Coffin, M., Wallace, P., & Weis, D. (2003). Leg 183 synthesis: Kerguelen Plateau-Broken ridge-a large igneous province. In *Proceedings of the ODP, Sci. Results, 183: College Station, TX (Ocean Drilling Program)* (pp. 1–48). https://doi.org/10.2973/odp.proc.sr.183.015.2003

GEBCO, C. G. (2023). GEBCO 2023 grid. In *British oceanographic data centre*. National Oceanography Centre, NERC.

Geoffroy, L. (2005). Volcanic passive margins. *Comptes Rendus Geoscience*, *337*(16), 1395–1408. https://doi.org/10.1016/j.crte.2005.10.006

Gibbs, A. (1984). Structural evolution of extensional basin margins. *Journal of the Geological Society*, *141*(4), 609–620. https://doi.org/10.1144/gsjgs.141.4.0609

Gillard, M., Autin, J., Manatschal, G., Sauter, D., Munschy, M., & Schaming, M. (2015). Tectonomagmatic evolution of the final stages of rifting along the deep conjugate Australian-Antarctic magma-poor rifted margins: Constraints from seismic observations. *Tectonics*, *34*(4), 753–783. https://doi.org/10.1002/2015TC003850

Gladczenko, T. P., & Coffin, M. F. (2001). Kerguelen Plateau crustal structure and basin formation from seismic and gravity data. *Journal of Geophysical Research*, *106*(B8), 16583–16601. https://doi.org/10.1029/2001jb000370

Gohl, K., Uenzelmann-Neben, G., & Grobys, N. (2011). Growth and dispersal of a Southeast African large igneous province. *South African Journal of Geology*, *114*(3–4), 379–386. https://doi.org/10.2113/gssajg.114.3-4.379

Graça, M. C., Kusznir, N., & Stanton, N. S. G. (2019). Crustal thickness mapping of the central south Atlantic and the geodynamic development of the Rio Grande Rise and Walvis Ridge. *Marine and Petroleum Geology*, *101*, 230–242. https://doi.org/10.1016/j.marpetgeo.2018.12.011

Gresseth, J. L. S., Osmundsen, P. T., & Péron-Pinvidic, G. (2023). 3D evolution of detachment fault systems in necking domains: Insights from the Klakk Fault Complex and the Frøya High, mid-Norwegian rifted margin. *Tectonics*, *42*(3), e2022TC007600. https://doi.org/10.1029/2022TC007600

Griffiths, R., & Campbell, I. (1991). Interaction of mantle plume heads with the Earth's surface and onset of small-scale convection. *Journal of Geophysical Research*, *96*(B11), 18295–18310. https://doi.org/10.1029/91jb01897

Harding, T. P. (1985). Seismic characteristics and identification of negative flower structures, positive flower structures, and positive structural inversion. *AAPG Bulletin*, *69*(4), 582–600. https://doi.org/10.1306/ad462538-16f7-11d7-8645000102c1865d

Hartley, R. A., Roberts, G. G., White, N., & Richardson, C. (2011). Transient convective uplift of an ancient buried landscape. *Nature Geoscience*, *4*(8), 562–565. https://doi.org/10.1038/ngeo1191

Hill, R., Campbell, I., Davies, G., & Griffiths, R. (1992). Mantle plumes and continental tectonics. *Science*, *256*(5054), 186–193. https://doi.org/10.1126/science.256.5054.186

Hinz, K. (1981). A hypothesis on terrestrial catastrophies Wedges of very thick oceanward dipping layers beneath passive continental margins. Their origin and paleoenvironmental significance. *Geologisches Jahrbuch Reihe E, Geophysik*, *22*, 3–28.

Hochmuth, K., Gohl, K., & Uenzelmann-Neben, G. (2015). Playing jigsaw with large igneous provinces—A plate tectonic reconstruction of Ontong Java Nui, West Pacific. *Geochemistry, Geophysics, Geosystems*, *16*(11), 3789–3807. https://doi.org/10.1002/2015GC006036

Hochmuth, K., Gohl, K., Uenzelmann-Neben, G., & Werner, R. (2019). Multiphase magmatic and tectonic evolution of a large igneous province-Evidence from the crustal structure of the Manihiki Plateau, western Pacific. *Tectonophysics*, *750*, 434–457. https://doi.org/10.1016/j.tecto.2018.11.014

Houtz, R. E., Hayes, D. E., & Markl, R. G. (1977). Kerguelen Plateau bathymetry, sediment distribution and crustal structure. *Marine Geology*, *25*(1–3), 95–130. https://doi.org/10.1016/0025-3227(77)90049-4

Hoyer, P. A., Haase, K. M., Regelous, M., O'Connor, J. M., Homrighausen, S., Geissler, W. H., & Jokat, W. (2022). Mantle plume and rift-related volcanism during the evolution of the Rio Grande Rise. *Communications Earth & Environment*, *3*(1), 1–10. https://doi.org/10.1038/s43247-022-00349-1

Huang, L., & Liu, C. y. (2017). Three types of flower structures in a divergent-wrench fault zone. *Journal of Geophysical Research: Solid Earth*, *122*(12), 10-478–10-497. https://doi.org/10.1002/2017jb014675

Inoue, H., Coffin, M. F., Nakamura, Y., Mochizuki, K., & Kroenke, L. W. (2008). Intrabasement reflections of the Ontong Java Plateau: Implications for plateau construction. *Geochemistry, Geophysics, Geosystems*, *9*(4), 1–19. https://doi.org/10.1029/2007GC001780

Jiang, Q., Jourdan, F., Olierook, H. K., Merle, R. E., & Whittaker, J. M. (2021). Longest continuously erupting large igneous province driven by plume-ridge interaction. *Geology*, *49*(2), 206–210. https://doi.org/10.1130/G47850.1

Karner, G. D., & Driscoll, N. W. (1993). Rift flank topography and extensional basin architecture: Formation of Broken Ridge, southeast Indian Ocean. *Anais-Academia Brasileira De Ciencias*, *65*, 263.

Kennett, J. P. (1977). Cenozoic evolution of Antarctic glaciation, the circum-Antarctic Ocean, and their impact on global paleoceanography. *Journal of Geophysical Research*, *82*(27), 3843–3860. https://doi.org/10.1029/jc082i027p03843

Khogenkumar, S., Nair, N., & Pandey, D. K. (2022). Off-sequence plume magmatism near Ninetyeast Ridge in the Indian Ocean: Evidence for extensive lateral flow of the Kerguelen plume. *Journal of the Geological Society*, *179*(6), jgs2021-2127. https://doi.org/10.1144/jgs2021-127

Koppers, A. A., Becker, T. W., Jackson, M. G., Konrad, K., Müller, R. D., Romanowicz, B., et al. (2021). Mantle plumes and their role in Earth processes. *Nature Reviews Earth & Environment*, *2*(6), 382–401. https://doi.org/10.1038/s43017-021-00168-6

Larsen, P.-H. (1988). Relay structures in a Lower Permian basement-involved extension system, East Greenland. *Journal of Structural Geology*, *10*(1), 3–8. https://doi.org/10.1016/0191-8141(88)90122-8

Lavier, L. L., & Manatschal, G. (2006). A mechanism to thin the continental lithosphere at magma-poor margins. *Nature*, *440*(7082), 324–328. https://doi.org/10.1038/nature04608

Lavier, L. L., Roger Buck, W., & Poliakov, A. N. (1999). Self-consistent rolling-hinge model for the evolution of large-offset low-angle normal faults. *Geology*, *27*(12), 1127–1130. https://doi.org/10.1130/0091-7613(1999)027<1127:SCRHMF>2.3.CO;2

Leitchenkov, G., Guseva, Y. B., Gandyukhin, V., Ivanov, S., & Safonova, L. (2014). Structure of the Earth's crust and tectonic evolution history of the Southern Indian Ocean (Antarctica). *Geotectonics*, *48*(1), 8–28. https://doi.org/10.1134/s001685211401004x

Lister, G., Etheridge, M., & Symonds, P. (1986). Detachment faulting and the evolution of passive continental margins. *Geology*, *14*(3), 246–250. https://doi.org/10.1130/0091-7613(1986)14<246:dfateo>2.0.co;2

Lister, G., Etheridge, M., & Symonds, P. (1991). Detachment models for the formation of passive continental margins. *Tectonics*, *10*(5), 1038–1064. https://doi.org/10.1029/90tc01007

MacKenzie, K., Orcutt, J., & McClain, J. (1980). Crustal structure of the Broken Ridge. *Eos, Transactions, American Geophysical Union*, *61*(46), 1049.

Mahoney, J., Macdougall, J., Lugmair, G., & Gopalan, K. (1983). Kerguelen hotspot source for Rajmahal traps and Ninetyeast Ridge? *Nature*, *303*(5916), 385–389. https://doi.org/10.1038/303385a0

Manatschal, G. (2004). New models for evolution of magma-poor rifted margins based on a review of data and concepts from West Iberia and the Alps. *International Journal of Earth Sciences*, *93*(3), 432–466. https://doi.org/10.1007/s00531-004-0394-7

Mann, P., Hempton, M. R., Bradley, D. C., & Burke, K. (1983). Development of pull-apart basins. *The Journal of Geology*, *91*(5), 529–554. https://doi.org/10.1086/628803

Markl, R. G. (1973). To Kerguelen Plateau and southeast Indian Rise. *Antarctic Journal of the United States*, *8*, 6.

Matthews, K. J., Seton, M., & Müller, R. D. (2012). A global-scale plate reorganization event at 105−100 Ma. *Earth and Planetary Science Letters*, *355*, 283–298. https://doi.org/10.1016/j.epsl.2012.08.023

McKenzie, D. (1978). Some remarks on the development of sedimentary basins. *Earth and Planetary Science Letters*, *40*(1), 25–32. https://doi.org/10.1016/0012-821x(78)90071-7

McNutt, M., Fischer, K., Kruse, S., & Natland, J. (1989). The origin of the Marquesas fracture zone ridge and its implications for the nature of hot spots. *Earth and Planetary Science Letters*, *91*(3–4), 381–393. https://doi.org/10.1016/0012-821x(89)90012-5

Miller, K. G., Browning, J. V., Schmelz, W. J., Kopp, R. E., Mountain, G. S., & Wright, J. D. (2020). Cenozoic sea-level and cryospheric evolution from deep-sea geochemical and continental margin records. *Science Advances*, *6*(20), eaaz1346. https://doi.org/10.1126/sciadv.aaz1346

Müller, R. D., Royer, J.-Y., & Lawver, L. A. (1993). Revised plate motions relative to the hotspots from combined Atlantic and Indian Ocean hotspot tracks. *Geology*, *21*(3), 275–278. https://doi.org/10.1130/0091-7613(1993)021<0275:rpmrtt>2.3.co;2

Munschy, M. (1998). La zone de Diamantine, temoin de la separation de l'Australie et de l'Antarctique: Arguments geophysiques. *Comptes Rendus de l'Academie des Sciences-Series IIA-Earth and Planetary Science*, *327*(8), 533–540. https://doi.org/10.1016/s1251-8050(99)80035-4

Munschy, M., Dyment, J., Boulanger, M. O., Boulanger, D., Tissot, J. D., Schlich, R., et al. (1992). Breakup and seafloor spreading between the Kerguelen Plateau-Labuan Basin and the Broken Ridge-Diamantina zone. In *Proceedings of the ODP, Science Results, 120: College Station, TX (Ocean Drilling Program)* (pp. 931–944). https://doi.org/10.2973/odp.proc.sr.120.123.1992

Munschy, M., Fritsch, B., Schlich, R., Fezga, F., Rotstein, Y., & Coffin, M. F. (1992). Structure and evolution of the central Kerguelen Plateau deduced from seismic stratigraphic studies and drilling at Site 747. In *Proceedings of the ODP, Science Results, 120: College Station, TX (Ocean Drilling Program)* (pp. 881–893). https://doi.org/10.2973/odp.proc.sr.120.125.1992

Munschy, M., Rotstein, Y., Schlich, R., & Coffin, M. F. (1993). Structure and tectonic setting of the 77 E and 75 E grabens, Kerguelen Plateau, south Indian Ocean. *Journal of Geophysical Research*, *98*(B4), 6367–6382. https://doi.org/10.1029/92jb02694

Munschy, M., & Schlich, R. (1987). Structure and evolution of the Kerguelen-Heard Plateau (Indian Ocean) deduced from seismic stratigraphy studies. *Marine Geology*, *76*, 131–152. https://doi.org/10.1016/0025-3227(87)90022-3

Mutter, J. C., & Cande, S. C. (1983). The early opening between broken Ridge and Kerguelen Plateau. *Earth and Planetary Science Letters*, *65*(2), 369–376. https://doi.org/10.1016/0012-821x(83)90174-7

Mutter, J. C., Talwani, M., & Stoffa, P. L. (1982). Origin of seaward-dipping reflectors in oceanic crust off the Norwegian margin by "subaerial sea-floor spreading". *Geology*, *10*(7), 353–357. https://doi.org/10.1130/0091-7613(1982)10<353:oosrio>2.0.co;2

Nakanishi, M., Sager, W. W., & Klaus, A. (1999). Magnetic lineations within Shatsky Rise, northwest Pacific Ocean: Implications for hot spot-triple junction interaction and oceanic plateau formation. *Journal of Geophysical Research*, *104*(B4), 7539–7556. https://doi.org/10.1029/1999JB900002

Naliboff, J. B., Buiter, S. J., Péron-Pinvidic, G., Osmundsen, P. T., & Tetreault, J. (2017). Complex fault interaction controls continental rifting. *Nature Communications*, *8*(1), 1–9. https://doi.org/10.1038/s41467-017-00904-x

Neuharth, D., Brune, S., Wrona, T., Glerum, A., Braun, J., & Yuan, X. (2022). Evolution of rift systems and their fault networks in response to surface processes. *Tectonics*, *41*(3), e2021TC007166. https://doi.org/10.1029/2021TC007166

Norton, I., & Molnar, P. (1977). Implications of a revised fit between Australia and Antarctica for the evolution of the eastern Indian Ocean. *Nature*, *267*(5609), 338–340. https://doi.org/10.1038/267338a0

O'Neill, C., Müller, D., & Steinberger, B. (2005). On the uncertainties in hot spot reconstructions and the significance of moving hot spot reference frames. *Geochemistry, Geophysics, Geosystems*, *6*(4), 1–35. https://doi.org/10.1029/2004GC000784

Operto, S., & Charvis, P. (1995). Kerguelen Plateau: A volcanic passive margin fragment? *Geology*, *23*(2), 137–140. https://doi.org/10.1130/0091-7613(1995)023<0137:KPAVPM>2.3.CO;2

Operto, S., & Charvis, P. (1996). Deep structure of the southern Kerguelen Plateau (southern Indian Ocean) from ocean bottom seismometer wide-angle seismic data. *Journal of Geophysical Research*, *101*(B11), 25077–25103. https://doi.org/10.1029/96JB01758

Osmundsen, P., & Péron-Pinvidic, G. (2018). Crustal-scale fault interaction at rifted margins and the formation of domain-bounding breakaway complexes: Insights from offshore Norway. *Tectonics*, *37*(3), 935–964. https://doi.org/10.1002/2017TC004792

Parsiegla, N., Gohl, K., & Uenzelmann-Neben, G. (2008). The Agulhas Plateau: Structure and evolution of a large igneous province. *Geophysical Journal International*, *174*(1), 336–350. https://doi.org/10.1111/j.1365-246X.2008.03808.x

Peacock, D. C. P., & Sanderson, D. J. (1995). Strike-slip relay ramps. *Journal of Structural Geology*, *17*(10), 1351–1360. https://doi.org/10.1016/0191-8141(95)97303-w

Peirce, J., Weissel, J., Driscoll, N. W., & Karner, G. D. (1989). Stratigraphic and tectonic evolution of Broken Ridge from seismic stratigraphy and Leg 121 drilling. In *Proceedings of the ODP, Initial Reports, 121: College Station, TX (Ocean Drilling Program)*. https://doi.org/10.2973/odp.proc.ir.121.1989

Pérez-Gussinyé, M., Andrés-Martínez, M., Araújo, M., Xin, Y., Armitage, J., & Morgan, J. (2020). Lithospheric strength and rift migration controls on synrift stratigraphy and breakup unconformities at rifted margins: Examples from numerical models, the Atlantic and South China Sea margins. *Tectonics*, *39*(12), e2020TC006255. https://doi.org/10.1029/2020TC006255

Peron-Pinvidic, G., & Manatschal, G. (2019). Rifted margins: State of the art and future challenges. *Frontiers in Earth Science*, *7*, 218. https://doi.org/10.3389/feart.2019.00218

Peron-Pinvidic, G., Manatschal, G., & Osmundsen, P. T. (2013). Structural comparison of archetypal Atlantic rifted margins: A review of observations and concepts. *Marine and Petroleum Geology*, *43*, 21–47. https://doi.org/10.1016/j.marpetgeo.2013.02.002

Peron-Pinvidic, G., & Osmundsen, P. T. (2018). The Mid Norwegian-NE Greenland conjugate margins: Rifting evolution, margin segmentation, and breakup. *Marine and Petroleum Geology*, *98*, 162–184. https://doi.org/10.1016/j.marpetgeo.2018.08.011

Picard, K., Brooke, B. P., Harris, P. T., Siwabessy, P. J., Coffin, M. F., Tran, M., et al. (2018). Malaysia Airlines flight MH370 search data reveal geomorphology and seafloor processes in the remote southeast Indian Ocean. *Marine Geology*, *395*, 301–319. https://doi.org/10.1016/j.margeo.2017.10.014

Pietsch, R., & Uenzelmann-Neben, G. (2015). The Manihiki Plateau—A multistage volcanic emplacement history. *Geochemistry, Geophysics, Geosystems*, *16*(8), 2480–2498. https://doi.org/10.1002/2015GC005852

Pindell, J., Graham, R., & Horn, B. (2014). Rapid outer marginal collapse at the rift to drift transition of passive margin evolution, with a Gulf of Mexico case study. *Basin Research*, *26*(6), 701–725. https://doi.org/10.1111/bre.12059

Planke, S., Symonds, P. A., Alvestad, E., & Skogseid, J. (2000). Seismic volcanostratigraphy of large-volume basaltic extrusive complexes on rifted margins. *Journal of Geophysical Research*, *105*(B8), 19335–19351. https://doi.org/10.1029/1999jb900005

Ramsay, D., Colwell, J., Coffin, M., Davies, H., Hill, P., Pigram, C., & Stagg, H. (1986). New findings from the Kerguelen Plateau. *Geology*, *14*(7), 589–593. https://doi.org/10.1130/0091-7613(1986)14<589:nfftkp>2.0.co;2

Reston, T. (2009). The structure, evolution and symmetry of the magma-poor rifted margins of the North and central Atlantic: A synthesis. *Tectonophysics*, *468*(1–4), 6–27. https://doi.org/10.1016/j.tecto.2008.09.002

Roberts, D. G. (1975). Marine geology of the Rockall Plateau and trough. *Philosophical Transactions of the Royal Society of London. Series A, Mathematical and Physical Sciences*, *278*(1285), 447–509.

Rotstein, Y., Munschy, M., Schlich, R., & Hill, P. J. (1991). Structure and early history of the Labuan Basin south Indian ocean. *Journal of Geophysical Research*, *96*(B3), 3887–3904. https://doi.org/10.1029/90jb01872

Rotstein, Y., Schlich, R., Munschy, M., & Coffin, M. F. (1992). Structure and tectonic history of the southern Kerguelen Plateau (Indian Ocean) deduced from seismic reflection data. *Tectonics*, *11*(6), 1332–1347. https://doi.org/10.1029/91tc02909

Royer, J.-Y., & Coffin, M. F. (1992). Jurassic to Eocene plate tectonic reconstruction in the Kerguelen Plateau region. In *Proceedings of the ODP, Science Results, 120: College Station, TX (Ocean Drilling Program)* (pp. 917–928). https://doi.org/10.2973/odp.proc.sr.120.200.1992

Sandiford, D., Brune, S., Glerum, A., Naliboff, J., & Whittaker, J. M. (2021). Kinematics of footwall exhumation at oceanic detachment faults: Solid-block rotation and apparent unbending. *Geochemistry, Geophysics, Geosystems*, *22*(4), e2021GC009681. https://doi.org/10.1029/2021GC009681

Sauermilch, I., Whittaker, J. M., Bijl, P. K., Totterdell, J., & Jokat, W. (2019). Tectonic, oceanographic, and climatic controls on the Cretaceous-Cenozoic sedimentary record of the Australian-Antarctic Basin. *Journal of Geophysical Research: Solid Earth*, *124*(8), 7699–7724. https://doi.org/10.1029/2018JB016683

Schaming, M., & Rotstein, Y. (1990). Basement reflectors in the Kerguelen Plateau, south Indian Ocean: Indications for the structure and early history of the plateau. *Geological Society of America Bulletin*, *102*(5), 580–592. https://doi.org/10.1130/0016-7606(1990)102<0580:britkp>2.3.co;2

Schierjott, J. C., Ito, G., Behn, M. D., Tian, X., Morrow, T., Kaus, B. J., & Escartín, J. (2023). How transform fault shear influences where detachment faults form near mid-ocean ridges. *Scientific Reports*, *13*(1), 9259. https://doi.org/10.1038/s41598-023-35714-3

Schlich, R., Munschy, M., Boulanger, D., Cantin, B., Coffin, M., Durand, J., et al. (1988). Résultats préliminaires de la campagne océanographique de sismique reflexion multitraces MD 47 dans le domaine sud du plateau de Kerguelen. *Comptes Rendus de l'Académie des Sciences-Series IIB-Mechanics-Physics-Astronomy*, *306*, 635–642.

Schlich, R., Rotstein, Y., & Schaming, M. (1993). Dipping basement reflectors along volcanic passive margins—New insight using data from the Kerguelen Plateau. *Terra Nova*, *5*(2), 157–163. https://doi.org/10.1111/j.1365-3121.1993.tb00241.x

Schlich, R., Wise, S., & Coffin, M. (1989). Central Kerguelen Plateau: Covering Leg 120. In *Proceedings of the ODP, Initial Reports, 120: College Station, TX (Ocean Drilling Program)*.

Ségoufin, J., Munschy, M., Bouysse, P., Mendel, V., Grikurov, G., Leitchenkov, G., et al. (2004). *Map of the Indian Ocean (1: 20 000 000), sheet 1:"Physiography", sheet 2:"Structural map"*. CGMW Edition.

Stagg, H. M. J., Colwell, J., Direen, N., O'Brien, P., Browning, B., Bernardel, G., et al. (2004). Geological framework of the continental margin in the region of the Australian Antarctic Territory. In *Geoscience Australia, Canberra, record 2004* (pp. 1–373).

Steinberger, B., & O'Connell, R. J. (1998). Advection of plumes in mantle flow: Implications for hotspot motion, mantle viscosity and plume distribution. *Geophysical Journal International*, *132*(2), 412–434. https://doi.org/10.1046/j.1365-246x.1998.00447.x

Sutra, E., & Manatschal, G. (2012). How does the continental crust thin in a hyperextended rifted margin? Insights from the Iberia margin. *Geology*, *40*(2), 139–142. https://doi.org/10.1130/G32786.1

Tikku, A. A., & Cande, S. C. (1999). The oldest magnetic anomalies in the Australian-Antarctic Basin: Are they isochrons? *Journal of Geophysical Research*, *104*(B1), 661–677. https://doi.org/10.1029/1998JB900034

Tikku, A. A., & Cande, S. C. (2000). On the fit of broken Ridge and Kerguelen Plateau. *Earth and Planetary Science Letters*, *180*(1–2), 117–132. https://doi.org/10.1016/s0012-821x(00)00157-6

Tomasi, S., Kusznir, N., Manatschal, G., & Despinois, F. (2021). The challenge in restoring magma-rich rifted margins: The example of the Mozambique-Antarctica conjugate margins. *Gondwana Research*, *95*, 29–44. https://doi.org/10.1016/j.gr.2021.03.009

Totterdell, J., Blevin, J., Struckmeyer, H., Bradshaw, B., Colwell, J., & Kennard, J. (2000). A new sequence framework Forthe Great Australian Bight: Starting with a Clean slate. *The APPEA Journal*, *40*(1), 95–118. https://doi.org/10.1071/aj99007

Tugend, J., Manatschal, G., Kusznir, N., Masini, E., Mohn, G., & Thinon, I. (2014). Formation and deformation of hyperextended rift systems: Insights from rift domain mapping in the Bay of Biscay-Pyrenees. *Tectonics*, *33*(7), 1239–1276. https://doi.org/10.1002/2014TC003529

Uenzelmann-Neben, G. (2020). Kerguelen Plateau sediment Drift, seismic reflection profile AWI-20200001 [Dataset]. PANGAEA. https://doi.org/10.1594/PANGAEA.922556

Uenzelmann-Neben, G. (2021a). Kerguelen Plateau sediment Drift, seismic reflection profile AWI-20200002 [Dataset]. PANGAEA. https://doi.org/10.1594/PANGAEA.934739

Uenzelmann-Neben, G. (2021b). Kerguelen Plateau sediment Drift, seismic reflection profile AWI-20200003 [Dataset]. PANGAEA. https://doi.org/10.1594/PANGAEA.935731

Uenzelmann-Neben, G., Gohl, K., Ehrhardt, A., & Seargent, M. (1999). Agulhas Plateau, SW Indian Ocean: New evidence for excessive volcanism. *Geophysical Research Letters*, *26*(13), 1941–1944. https://doi.org/10.1029/1999gl900391

Versfelt, J., & Rosendahl, B. (1989). Relationships between pre-rift structure and rift architecture in Lakes Tanganyika and Malawi, East Africa. *Nature*, *337*(6205), 354–357. https://doi.org/10.1038/337354a0

Vine, F. J., & Matthews, D. H. (1963). Magnetic anomalies over oceanic ridges. *Nature*, *199*(4897), 947–949. https://doi.org/10.1038/199947a0

Walker, J. D., & Geissman, J. W. (2022). Geologic time scale v. 6.0: Geological Society of America. https://doi.org/10.1130/2022.CTS006C

Wallace, P. J., Frey, F. A., Weis, D., & Coffin, M. F. (2002). *Origin and evolution of the Kerguelen Plateau, broken Ridge and Kerguelen archipelago* (Vol. 43, pp. 1105–1108). Oxford University Press.

Webber, S., Norton, K., Little, T., Wallace, L., & Ellis, S. (2018). How fast can low-angle normal faults slip? Insights from cosmogenic exposure dating of the active Mai'iu fault, Papua New Guinea. *Geology*, *46*(3), 227–230. https://doi.org/10.1130/G39736.1

Weissel, J., Peirce, J., Taylor, E., & Alt, J. (1991). Age distribution of volcanism along aseismic ridges in the eastern Indian Ocean. In *Proceedings of the ODP, Science Results, 121: College Station, TX (Ocean Drilling Program)*. https://doi.org/10.2973/odp.proc.sr.121.1991

Weissel, J. K., & Karner, G. D. (1989). Flexural uplift of rift flanks due to mechanical unloading of the lithosphere during extension. *Journal of Geophysical Research*, *94*(B10), 13919–13950. https://doi.org/10.1029/jb094ib10p13919

Wernicke, B. (1981). Low-angle normal faults in the Basin and range province: Nappe tectonics in an extending orogen. *Nature*, *291*(5817), 645–648. https://doi.org/10.1038/291645a0

Wernicke, B., & Burchfiel, B. (1982). Modes of extensional tectonics. *Journal of Structural Geology*, *4*(2), 105–115. https://doi.org/10.1016/0191-8141(82)90021-9

Wessel, P., Luis, J., Uieda, L., Scharroo, R., Wobbe, F., Smith, W. H., & Tian, D. (2019). The generic mapping tools version 6 [Software]. Geochemistry, Geophysics, Geosystems, *20*, 5556–5564. https://doi.org/10.1029/2019GC00851511

White, R., & McKenzie, D. (1989). Magmatism at rift zones: The generation of volcanic continental margins and flood basalts. *Journal of Geophysical Research*, *94*(B6), 7685–7729. https://doi.org/10.1029/JB094iB06p07685

White, R. S., Spence, G. D., Fowler, S. R., McKenzie, D. P., Westbrook, G. K., & Bowen, A. N. (1987). Magmatism at rifted continental margins. *Nature*, *330*(6147), 439–444. https://doi.org/10.1038/330439a0

Whittaker, J., Muller, R., Leitchenkov, G., Stagg, H., Sdrolias, M., Gaina, C., & Goncharov, A. (2007). Major Australian-Antarctic plate reorganization at Hawaiian-Emperor bend time. *Science*, *318*(5847), 83–86. https://doi.org/10.1126/science.1143769

Whittaker, J. M., Afonso, J. C., Masterton, S., Müller, R. D., Wessel, P., Williams, S. E., & Seton, M. (2015). Long-term interaction between mid-ocean ridges and mantle plumes. *Nature Geoscience*, *8*(6), 479–483. https://doi.org/10.1038/ngeo2437

Whittaker, J. M., Williams, S. E., & Müller, R. D. (2013). Revised tectonic evolution of the eastern Indian ocean. *Geochemistry, Geophysics, Geosystems*, *14*(6), 1891–1909. https://doi.org/10.1002/ggge.20120

Williams, S. E., Whittaker, J. M., Granot, R., & Müller, D. R. (2013). Early India-Australia spreading history revealed by newly detected Mesozoic magnetic anomalies in the Perth Abyssal Plain. *Journal of Geophysical Research: Solid Earth*, *118*(7), 3275–3284. https://doi.org/10.1002/jgrb.50239

Wise, S. W., Breza, J. R., Harwood, D. M., Wei, W., & Zachos, J. C. (1992). Paleogene glacial history of Aantarctica in light of Leg 120 drilling results. In *Proceedings of the ODP, Science Results, 121: College Station, TX (Ocean Drilling Program)* (pp. 1001–1030). https://doi.org/10.2973/odp.proc.sr.120.205.1992

Zhang, J., Sager, W. W., & Korenaga, J. (2015). The Shatsky Rise oceanic plateau structure from two-dimensional multichannel seismic reflection profiles and implications for oceanic plateau formation. In *Special paper of the Geological Society of America* (Vol. 511, pp. 103–126). https://doi.org/10.1130/2015.2511(06)

References From the Supporting Information

Uenzelmann-Neben, G., & Westerhold, T. (2020). Kerguelen Plateau drift deposits: Outstanding high-resolution chronicle of Cenozoic climatic and oceanographic changes in the southern Indian ocean. Bonn. In *Gutachterpanel Forschungsschiffe* (pp. 1–92). https://doi.org/10.2312/cr_so272

Yilmaz, O. (2001). *Seismic data analysis: Processing, inversion, and interpretation of seismic data* (p. 2065). Society of Exploration Geophysicists.